

**Electronic Supporting Information For:**

**Tetrabenzo[b,de,gh,j][1,10]phenanthroline: a nitrogen-  
doped nanographene as a selective metal cation and  
proton fluorophore**

Xiao Xu,<sup>a,b</sup> Ting Xia,<sup>a,b</sup> Xu-Lang Chen,<sup>b,c</sup> Xiang Hao,<sup>d</sup> Tongling Liang,<sup>d</sup> Huan-Rong  
Li<sup>\*a</sup> and Han-Yuan Gong<sup>\*b</sup>

[a] Department of Chemistry, Renmin University of China, No. 59, Zhongguancun St, HaiDian District, Beijing 100872, China.

[b] College of Chemistry, Beijing Normal University, No. 19, XinJieKouWai St, HaiDian District, Beijing 100875, China.

[c] College of Chemistry and Chemical Engineering, Hubei Key Laboratory of Pollutant Analysis and Reuse Technology, Hubei Normal University, Huangshi 435002, China.

[d] Institute of Chemistry, Chinese Academy of Sciences, Beijing 100190, P. R. China; University of Chinese Academy of Sciences, Beijing 100049, China

\*Correspondence: [hrli@ruc.edu.cn](mailto:hrli@ruc.edu.cn) (H.-R. L.); [hanyuangong@bnu.edu.cn](mailto:hanyuangong@bnu.edu.cn) (H.-Y.G.)

## Table of Contents

**Section S1:** *General considerations (pp. S3)*

**Section S2:** *Synthesis and characterization of Tetrabenzob[b,de,gh,j][1,10]phenanthroline (TB(phen)) (pp. S4-S13)*

**Section S3:** *Metal cation coordination study of TB(phen) in THF/CH<sub>3</sub>OH (1:1, v/v) (pp. S14-S38)*

**Section S4:** *Single crystals X-ray diffraction analyses of [(TB(phen))<sub>2</sub>•Cu<sup>+</sup>]•CF<sub>3</sub>SO<sub>3</sub><sup>-</sup>•THF, [(TB(phen))<sub>2</sub>•Ag<sup>+</sup>]•PF<sub>6</sub><sup>-</sup>•H<sub>2</sub>O and [TB(phen)•Cd<sup>2+</sup>•(NO<sub>3</sub><sup>-</sup>)<sub>2</sub>]•CH<sub>3</sub>OH (pp. S39-S42)*

**Section S5:** *Protonation study of TB(phen) in CH<sub>2</sub>Cl<sub>2</sub> (pp. S43-S44)*

**Section S6:** *Single crystal X-ray diffraction analysis of [TB(phen)•H<sup>+</sup>]•CF<sub>3</sub>SO<sub>3</sub><sup>-</sup> (pp. S45-S46)*

## *Section S1: General Considerations*

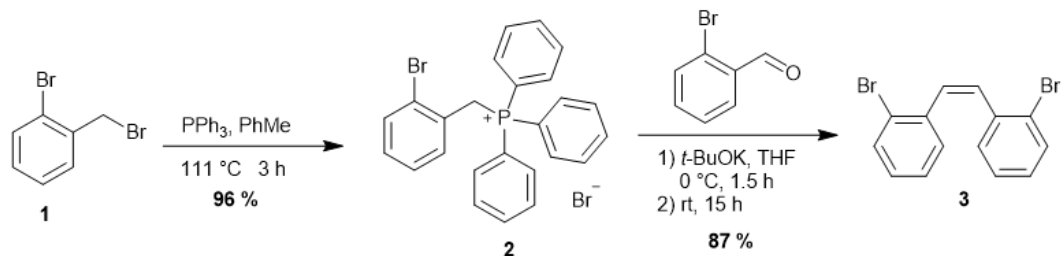
All solvents, reagents and all deuterated solvents were purchased from Innochem, Hwrk, Chem, Energy Chemical or Cambridge Isotope Laboratories commercial suppliers and used without further purification.  $^1\text{H}$  and  $^{13}\text{C}$  NMR spectra were recorded on 400 JNM-ECZ 400S or 600 JNM-ECZ 400S instrument. The  $^1\text{H}$  and  $^{13}\text{C}$  NMR chemical shifts are referenced to residual solvent signals ( $\text{CDCl}_3$ :  $\delta_{\text{H}} = 7.26$  ppm,  $\delta_{\text{C}} = 77.16$  ppm).<sup>1</sup> High resolution mass spectra (HMRS) were detected on AB SCIEX Triple TOF 56q00+ instrument. Uv-vis spectra were collected on a Shimadzu UV-2600 spectrometer. Fluorescence emission spectra were collected on an Edinburgh Instruments FS5 spectrometer. Fluorescence lifetimes ( $\tau$ ) were collected on an Edinburgh Instruments FS980. Fluorescence quantum yields were obtained using a HAMAMATSU Quantaaurus-QY instrument.

All single crystals used to obtain the X-ray diffraction structures reported in the text grew as yellow or red prism, green block or dark-orange plate. The .cif documents are available as the separate supporting information files, which provide details regarding the specific crystals used for the analysis, along with the structures in question. Diffraction grade crystals were obtained by slow evaporation from a mixture solution of  $\text{CH}_2\text{Cl}_2/\text{C}_2\text{H}_5\text{OH}$  or  $\text{THF}/\text{CH}_3\text{OH}$  as described below.

The crystals used for single crystal analyses were cut from clusters of the corresponding crystals and had the approximate dimensions given in the .cif documents. The data were collected on XtalLAB Synergy diffractor. Data reduction was performed using CrysAlispro (Rigaku OD) software packages. The structures were refined by full-matrix least-squares on F2 with anisotropic displacement parameters for the non-H atoms using SHELXL-2018/3.<sup>2-4</sup> Definitions used for calculating R(F),  $R_w(\text{F}2)$  and the goodness of fit, S, are given below and in the .cif documents.<sup>5</sup> Neutral atom scattering factors and values used to calculate the linear absorption coefficient are from the International Tables for X-ray Crystallography (1992).<sup>6</sup> All ellipsoid figures were generated using SHELXTL or Ortep software.<sup>7</sup> Tables of positional and thermal parameters, bond lengths and angles, torsion angles, figures and lists of observed and calculated structure factors are located in the corresponding .cif documents available from the Cambridge Crystallographic Centre and may be obtained by quoting the CCDC ref. numbers 2127677, 2127679, 2127693, 2127694 and 2127695. The .cif documents also contain details of the crystal data, data collection, and structure refinement for each structure.

**Section S2: Synthesis and characterization of tetrabenzob[*b,de,gh,j*][1,10]phenanthroline (TB(phen))**

**Synthesis of (Z)-2,2'-dibromo-stilbene 3<sup>8</sup>**



2-bromobenzyl bromide **1** (30.0 g, 120 mmol) and triphenylphosphine (31.8 g, 121 mmol) were added into a 500 mL three-necked round bottom flask. The flask was evacuated and backfilled with argon (Ar) for 3 times. Then 300 mL toluene was added and the mixture was then heated at 110 °C for 3 h under Ar atmosphere. After cooling to room temperature and then filtered, the filter residue was washed with petroleum ether (3 × 100 mL), which give out product **2** as white powder, which was directly carried to the next step without further purification.

Under the condition of Ar and ice bath, compound **2** (50.0 g, 115 mmol) and 900 mL anhydrous THF was added into a 2000 mL three-necked round bottom flask, then potassium *tert*-butoxide (14.0 g, 125 mmol) was added slowly, after stirring for 1.5 h, the reaction system turns orange-yellow. Then 2-bromobenzaldehyde (23.8 g, 129 mmol) in anhydrous THF (50 mL) was added in flask and continued to stir for 15 h. Then 30 mL water was carefully added to quench the reaction and stir for 15 min. Reaction mixture was treated with rotary evaporation to remove most of THF, then extract with CH<sub>2</sub>Cl<sub>2</sub> (3 × 100 mL). The organic layer was combined and dried over with anhydrous Na<sub>2</sub>SO<sub>4</sub>. Then the solvent was removed via rotary evaporator. The residues were separated and purified by column chromatography (silica gel, 200-300 mesh; elute as petroleum ether (PE; boiling range 60-90 °C)/DCM (20:1, *v/v*) to obtain compound **3** (34.0 g, yield 87%) as white solid. <sup>1</sup>H NMR (400 MHz, CDCl<sub>3</sub>) δ (ppm): 7.57 (d, *J* = 8.0 Hz, 2H), 7.08–6.95 (m, 6H), 6.78 (s, 2H).

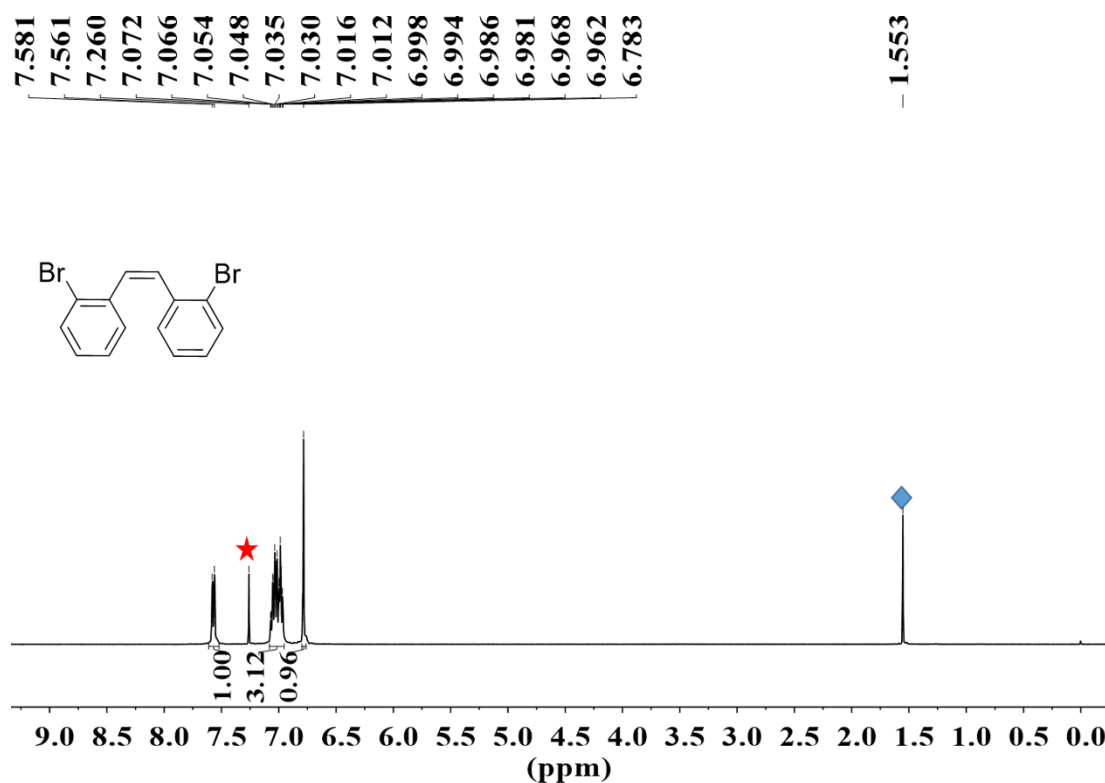
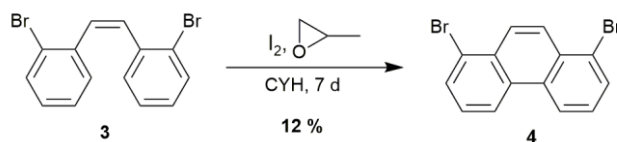


**Figure S1.**  $^1\text{H}$  NMR spectrum of **3** in  $\text{CDCl}_3$  at 298 K (400 MHz) (red “★” represents residual  $\text{CDCl}_3$ ; blue “◆” represents  $\text{H}_2\text{O}$ ).

### Synthesis of 1,8-dibromophenanthrene **4**<sup>9</sup>



(*Z*)-2,2'-dibromo-stilbene **3** (10.0 g, 29.6 mmol) was dissolved in 1000 mL cyclohexane in a 2000 mL quartz photochemical reaction vessel. Iodine (7.62 g, 30.0 mmol) was added and Ar was bubbled through the solution for 30 min, then propylene oxide (420 mL, 6.00 mol) was added. The solution was put in the photoreactor and irradiated with 1500W Hg arc lamp for 7 days. After the irradiation, evaporate the solvent, the resulting solid was filtered with suction to obtain compound **4** (1.20 g, yield 12%) as light yellow needle-like solid.  $^1\text{H}$  NMR (400 MHz,  $\text{CDCl}_3$ )  $\delta$  (ppm): 8.67 (d,  $J = 8.4$  Hz, 2H), 8.32 (s, 2H), 7.93 (d,  $J = 8.4$  Hz, 2H), 7.53 (t,  $J = 8.4$  Hz, 2H).

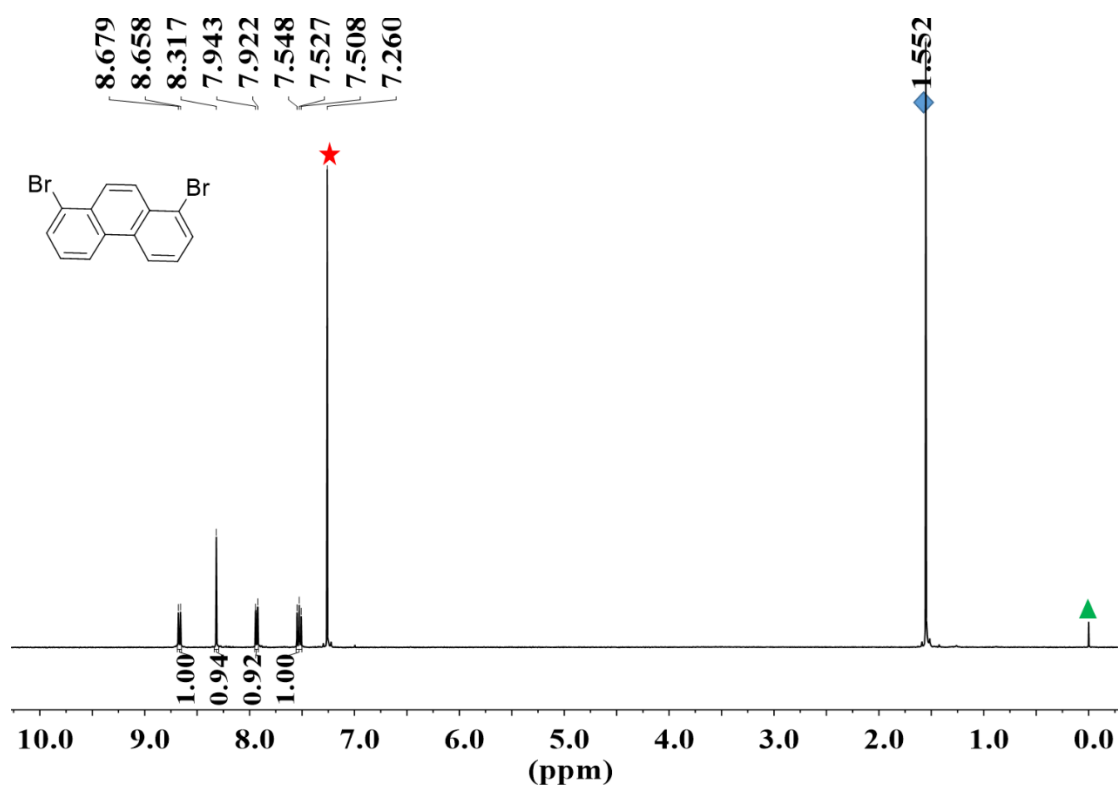
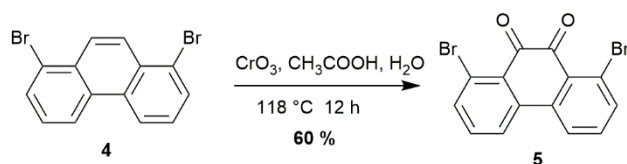


**Figure S2.** <sup>1</sup>H NMR spectrum of **4** in CDCl<sub>3</sub> at 298 K (400 MHz) (red “★” represents residual CDCl<sub>3</sub>; blue “◆” represents H<sub>2</sub>O; green “▲” represents TMS).

### Synthesis of 1,8-dibromophenanthrene-9,10-dione **5**<sup>10</sup>



Under the nitrogen atmosphere, 1,8-dibromophenanthrene **4** (5.00 g, 14.9 mmol) and 200 mL acetic acid were added in a 500 mL three-necked round bottom flask, the mixture was heated at 118 °C. Then CrO<sub>3</sub> (5.96 g, 59.6 mmol) was dissolved in 50 mL water and slowly drip into the reaction system. The solution was stirred for 12 h after the last addition, cooled to 70 °C, filter while hot, the crude product was obtained and washed with H<sub>2</sub>O/EtOH (1:1, v/v) for three times (3 × 100 mL). After drying, compound **5** (3.27 g, yield 60%) was achieved as an orange solid. <sup>1</sup>H NMR (400 MHz, CDCl<sub>3</sub>) δ (ppm): 7.93 (d, *J* = 8.0 Hz, 2H), 7.75 (d, *J* = 8.0 Hz, 2H), 7.52 (t, *J* = 8.4 Hz, 2H).

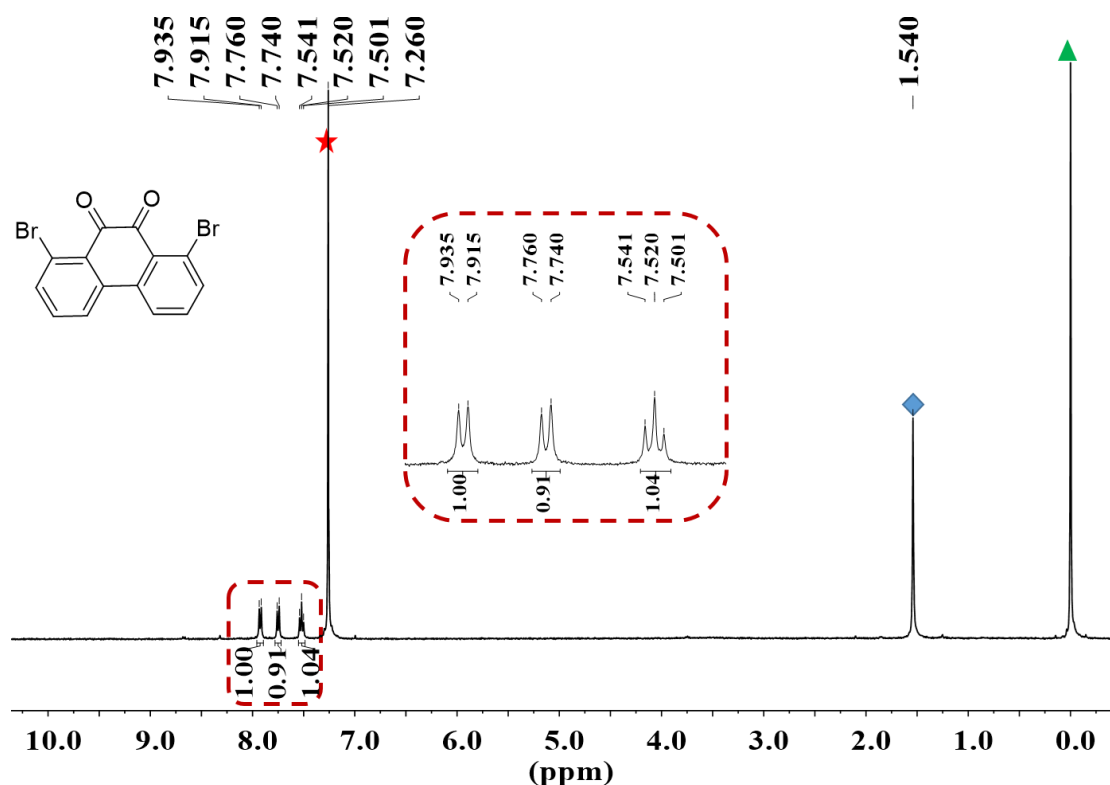
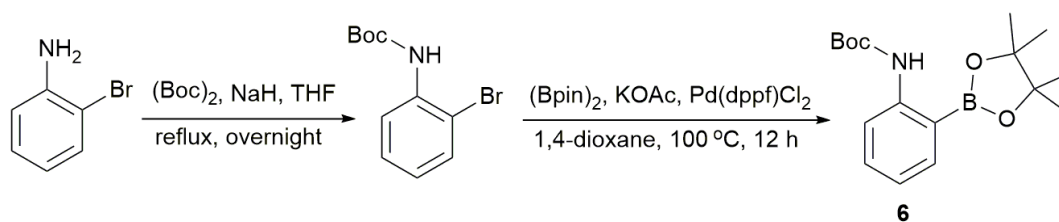


**Figure S3.**  $^1\text{H}$  NMR spectrum of **5** in  $\text{CDCl}_3$  at 298 K (400 MHz) (red “★” represents residual  $\text{CDCl}_3$ ; blue “◆” represents  $\text{H}_2\text{O}$ ; green “▲” represents TMS).

### Synthesis of tetramethylethylidene 2-[*N*-(*tert*-butoxycarbonyl)amino]phenylboronate **6**<sup>11</sup>



2-bromoaniline (8.60 g, 5.46 mL, 50.0 mmol) was added to a solution of sodium hydride (1.32 g, 55.0 mmol) in 300 mL THF under Ar atmosphere. The mixture was heated to reflux for 1 h and then cooled to room temperature. Then di-*tert*-butyl dicarbonate (13.1 g, 13.8 mL, 60.0 mmol) was added and the slurry was stirred for 1 h. A second portion of sodium hydride (1.32 g, 55.0 mmol) was added to the mixture and the reaction was refluxed for overnight. The reaction was cooled to room temperature and quenched with water carefully. Reaction mixture was treated with rotary evaporation to remove most of THF, then extracted with  $\text{CH}_2\text{Cl}_2$  ( $3 \times 100$  mL). The combined organic layers were washed with a saturated aqueous solution of  $\text{NH}_4\text{Cl}$  and

saturated aqueous solution of NaHCO<sub>3</sub>, then dried over anhydrous Na<sub>2</sub>SO<sub>4</sub>. The solvent was removed via rotary evaporator and the crude product was purified by flash chromatography (silica gel, 200-300 mesh; elute as petroleum ether (PE)/ethyl acetate (EA), 20:1, v/v) to afford 2-bromo-*N*-(*tert*-butoxycarbonyl)aniline (13.1 g, 96%) as orange liquid.

Under the nitrogen atmosphere, 2-bromo-*N*-(*tert*-butoxycarbonyl)aniline (2.72 g, 10.0 mmol), potassium acetate (4.41 g, 45.0 mmol), bis(pinacolato)diboron (3.05 g, 12.0 mmol), Pd(dppf)Cl<sub>2</sub> (366 mg, 0.5 mmol) and 150 mL 1,4-dioxane were added in a 250 mL three-necked flask. The reaction was heated to 100 °C and stirred overnight. The resulting suspension was cooled to room temperature. The solvent was removed via rotary evaporator and the residue was diluted with 25 mL CH<sub>2</sub>Cl<sub>2</sub> and filtered through celite and the filtrate was concentrated. The crude product was purified by column chromatography (silica gel, 200-300 mesh; elute as petroleum ether (PE)/ethyl acetate (EA), 15:1, v/v) to give compound **6** (1.60 g, yield 50%) as a white solid. <sup>1</sup>H NMR (400 MHz, CDCl<sub>3</sub>) δ (ppm): 8.68 (s, 1H), 8.17 (d, *J* = 8.4 Hz, 1H), 7.71 (dd, *J* = 7.2 Hz, *J* = 1.2 Hz, 1H), 7.42 (td, *J* = 7.2 Hz, *J* = 1.2 Hz, 1H), 6.98 (td, *J* = 7.2 Hz, *J* = 0.8 Hz, 1H), 1.52 (s, 9H), 1.36 (s, 12H).

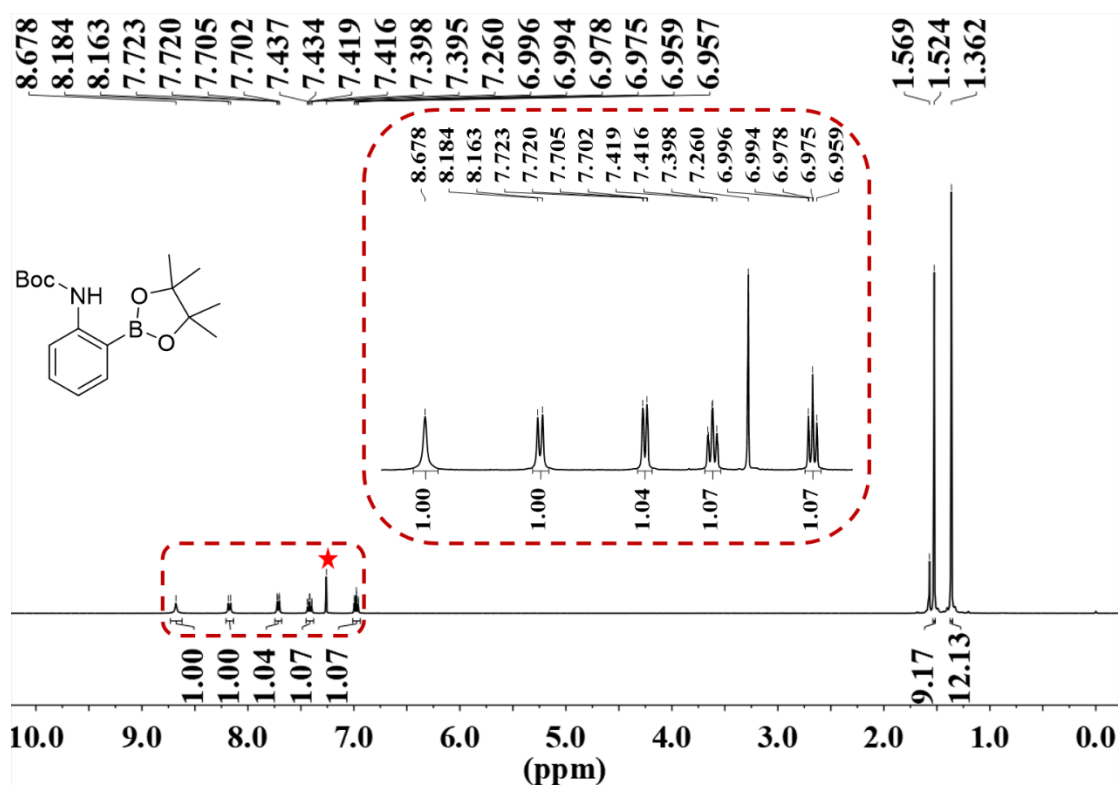
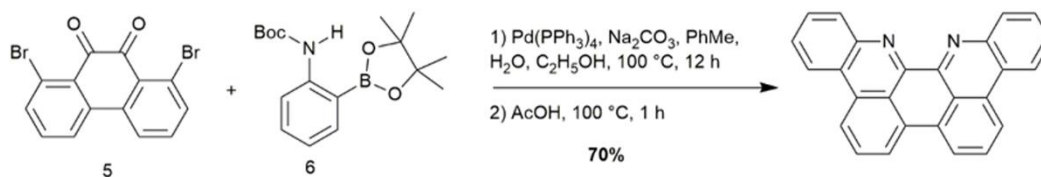


**Figure S4.** <sup>1</sup>H NMR spectrum of **6** in CDCl<sub>3</sub> at 298 K (400 MHz) (red “★” represents residual CDCl<sub>3</sub>).

## Synthesis of tetrabenzo[*b,de,gh,j*][1,10]phenanthroline (TB(phen))



Under anhydrous and Ar conditions, a 250 mL three-necked flask was charged with compound **5** (500 mg, 1.37 mmol), compound **6** (960 mg, 3.00 mmol), Pd(PPh<sub>3</sub>)<sub>4</sub> (162 mg, 0.140 mmol) and Na<sub>2</sub>CO<sub>3</sub> (652 mg, 6.15 mmol). Then 20 mL toluene, 1 mL water and 1 mL ethanol were added and the resulting mixture was heated to 100 °C for 12 h. The reaction was cooled to room temperature, exposed to air, then 100 mL glacial acetic acid was slowly added, and allowed to heat for an additional 1 h at 100 °C. The reaction mixture was cooled to room temperature, filtered through a short celite plug, trimethylamine was added to neutralize the solution, then washed with 50 mL water. The mixture was extracted with CH<sub>2</sub>Cl<sub>2</sub> (3 × 100 mL) and organic extracts were combined, dried over Na<sub>2</sub>SO<sub>4</sub>. The solvent was removed via rotary evaporator. The crude product was purified by flash column chromatography (neutral alumina; elute as CH<sub>2</sub>Cl<sub>2</sub>) to obtain **TB(phen)** (340 mg, yield 70%) as yellow powder. Mp > 365 °C. <sup>1</sup>H NMR (400 MHz, CDCl<sub>3</sub>) δ (ppm): 8.66 (t, *J* = 7.2 Hz, 4H), 8.62 (d, *J* = 8.0 Hz, 2H), 8.52 (d, *J* = 8.0 Hz, 2H), 7.96 (t, *J* = 8.0 Hz, 2H), 7.86 (m, 2H), 7.76 (m, 2H). <sup>13</sup>C NMR (600 MHz, CDCl<sub>3</sub>/TFA-*d* (4:1, v/v)) δ (ppm): 142.6, 138.3, 135.8, 135.4, 132.5, 131.8, 131.3, 126.3, 125.8, 125.6, 124.3, 123.5, 119.3. HRMS (ESI) *m/z*: [M + H]<sup>+</sup> calcd. for C<sub>26</sub>H<sub>15</sub>N<sub>2</sub> 355.1235, found 355.1225.

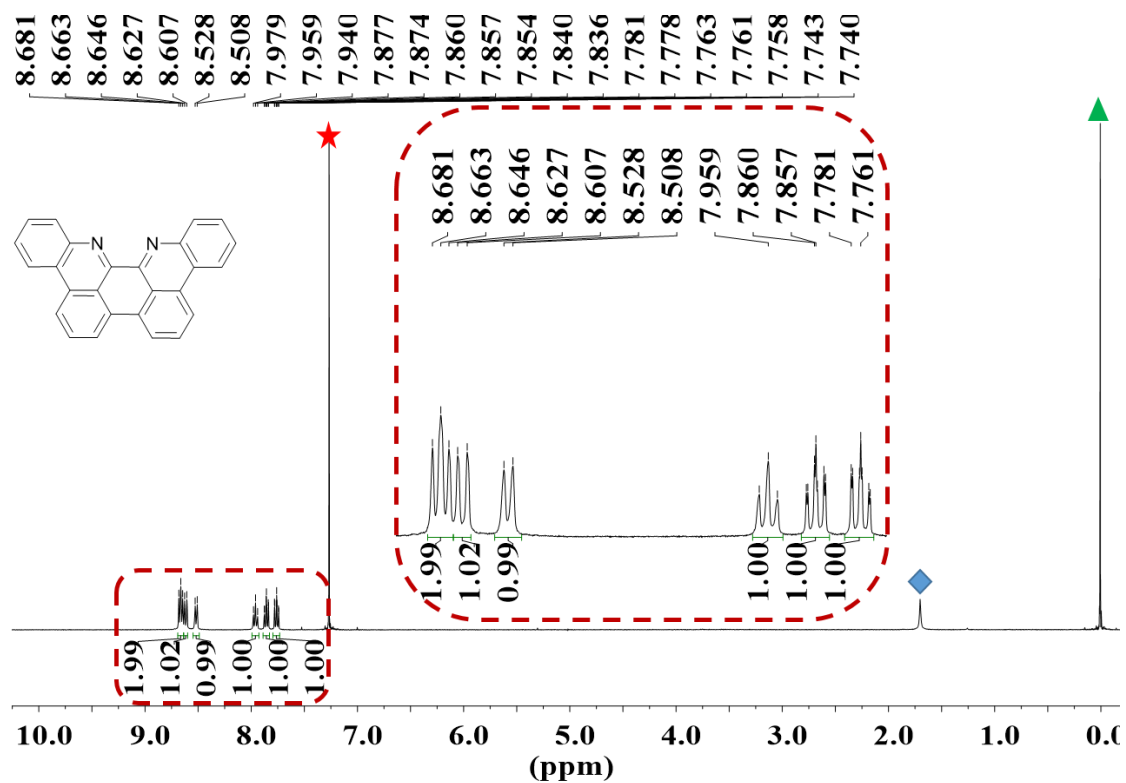


**Figure S5.**  $^1\text{H}$  NMR spectrum of TB(phen) in  $\text{CDCl}_3$  at 298 K (400 MHz) (red “★” represents residual  $\text{CDCl}_3$ ; blue “◆” represents  $\text{H}_2\text{O}$ ; green “▲” represents TMS).

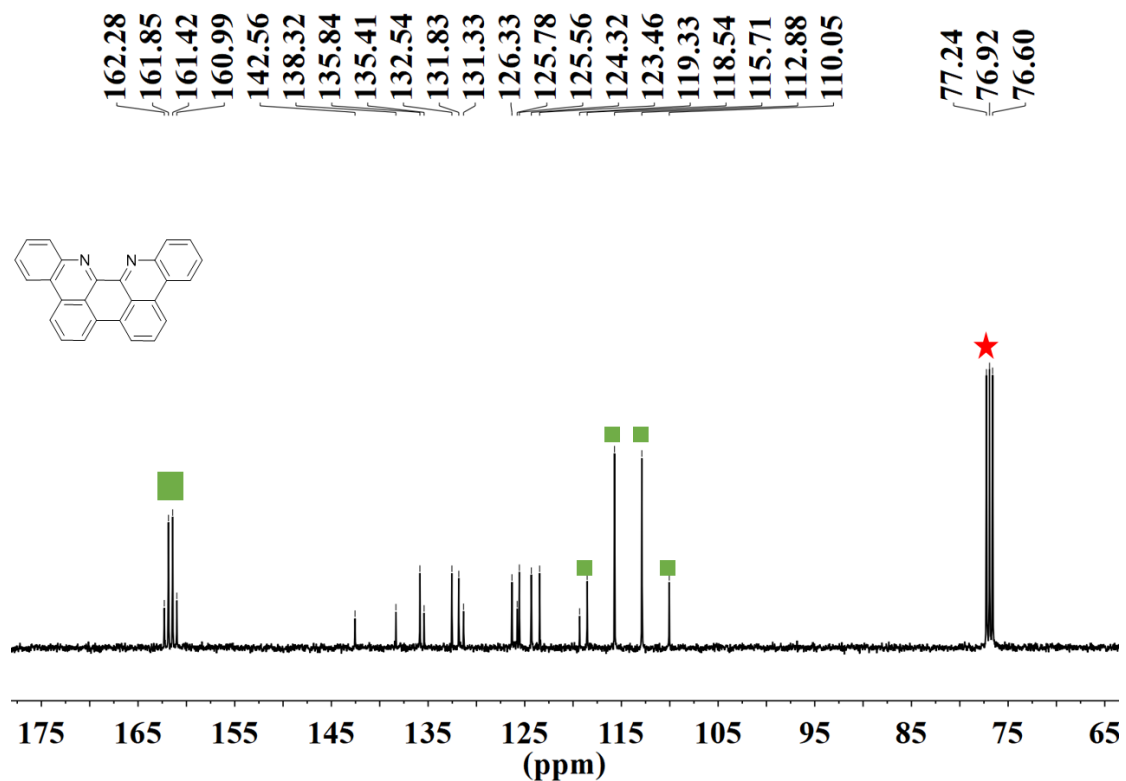


**Figure S6.**  $^{13}\text{C}$  NMR spectrum of TB(phen) in  $\text{CDCl}_3/\text{TFA-}d$  (4:1,  $v/v$ ) at 298 K (600 MHz) (red “★” represents residual  $\text{CDCl}_3$ ; green “■” represents residual TFA- $d$ ).

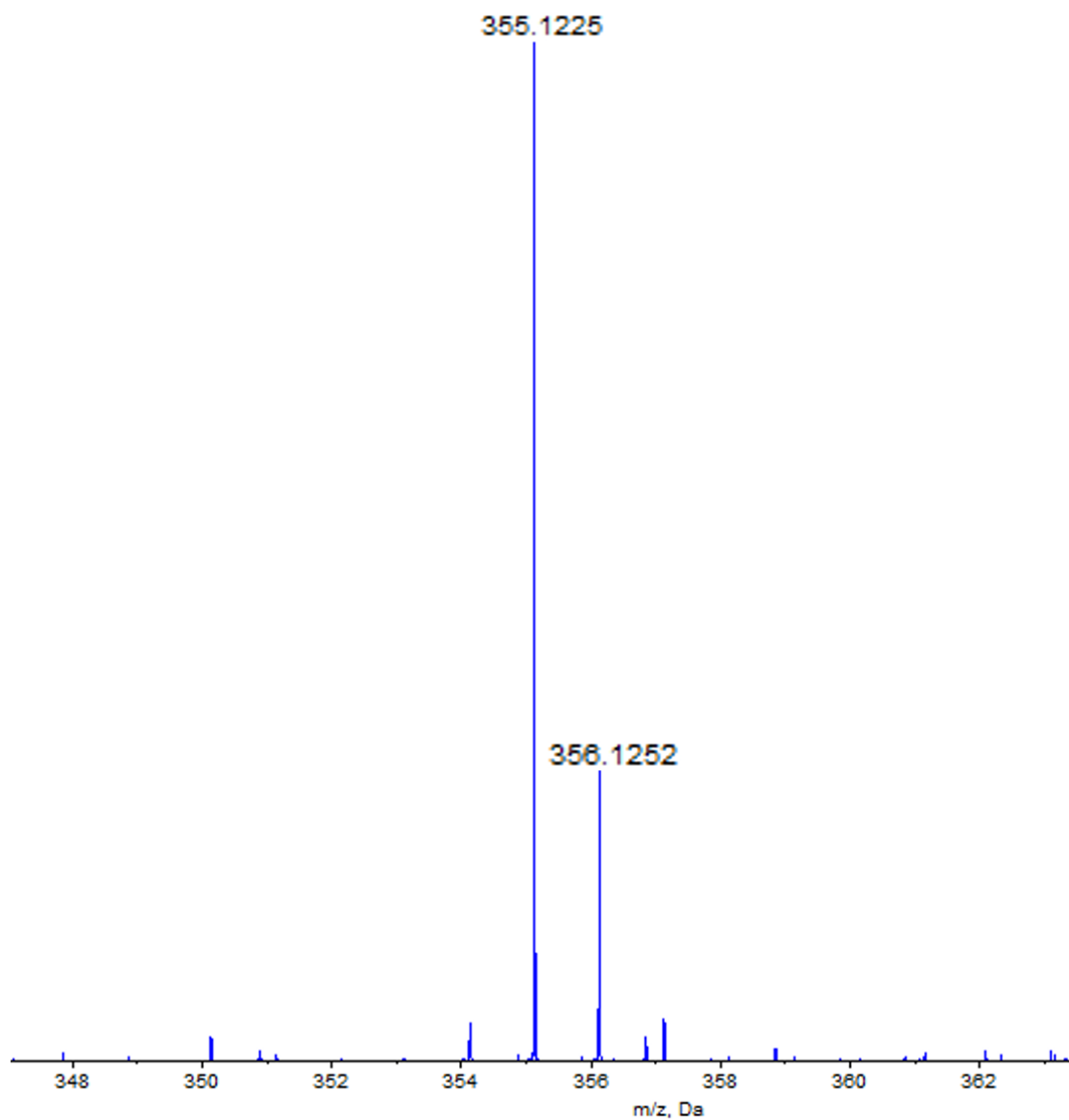


**Figure S7.** Positive ESI HRMS spectrum of **TB(phen)**.

Single crystal sample of [TB(phen)•C<sub>2</sub>H<sub>5</sub>OH] was cultivated via slow evaporation of the solution containing TB(phen) (2 mM) in CH<sub>2</sub>Cl<sub>2</sub>/C<sub>2</sub>H<sub>5</sub>OH (2:1, v/v).

**Table S1.** Single crystal X-ray diffraction data summary of [TB(phen)•C<sub>2</sub>H<sub>5</sub>OH].

	[TB(phen)•C <sub>2</sub> H <sub>5</sub> OH]
CCDC No.	2127677
description	prism
color	yellow
from solution	CH <sub>2</sub> Cl <sub>2</sub> /C <sub>2</sub> H <sub>5</sub> OH
empirical formula	C <sub>28</sub> H <sub>20</sub> N <sub>2</sub> O
<i>Mr</i>	400.46
crystal size (mm <sup>3</sup> )	0.20 × 0.10 × 0.05
Crystal system	orthorhombic
Space group	P 21 21 21
a [Å]	5.0045(10)
b [Å]	16.990(3)
c [Å]	22.671(5)
α [deg]	90.00
β [deg]	90.00
γ [deg]	90.00
V/ [Å <sup>3</sup> ]	1927.7(3)
d/[g/cm <sup>3</sup> ]	1.380
Z	4
T [K]	99.97(13)
R1, wR2 <i>I</i> > 2σ( <i>I</i> )	0.0471, 0.1081
R1, wR2 (all data)	0.0572, 0.1130
Quality of fit	1.013

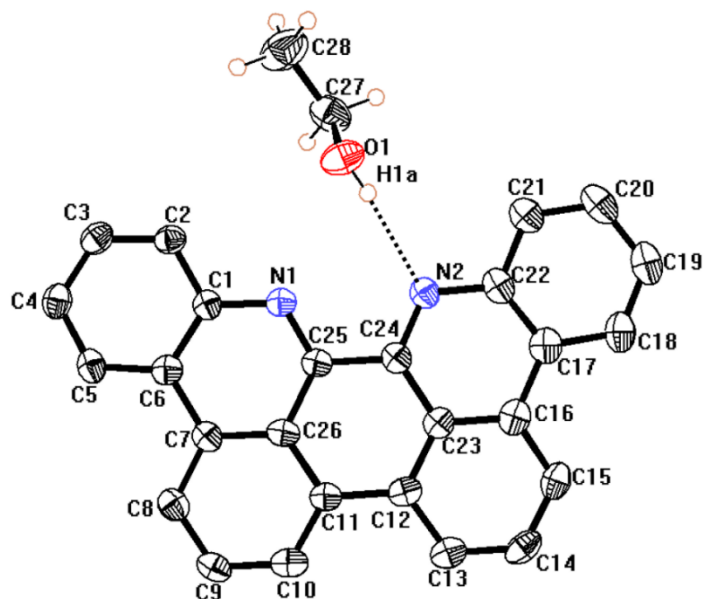


**Figure S8.** Ellipsoid form showing **TB(phen)** in the single crystal structure of **[TB(phen)•C<sub>2</sub>H<sub>5</sub>OH]**. Displacement ellipsoids are scaled to the 50% probability level. All the other H atoms have been omitted for clarity. Selected interatomic lengths (Å): N(2)...H(1a) 2.25(1), N(2)...O(1) 3.06(5). Selected interatomic angle:  $\angle$  O(1) ...H(1a) ...N(2) 173.6(1)°.

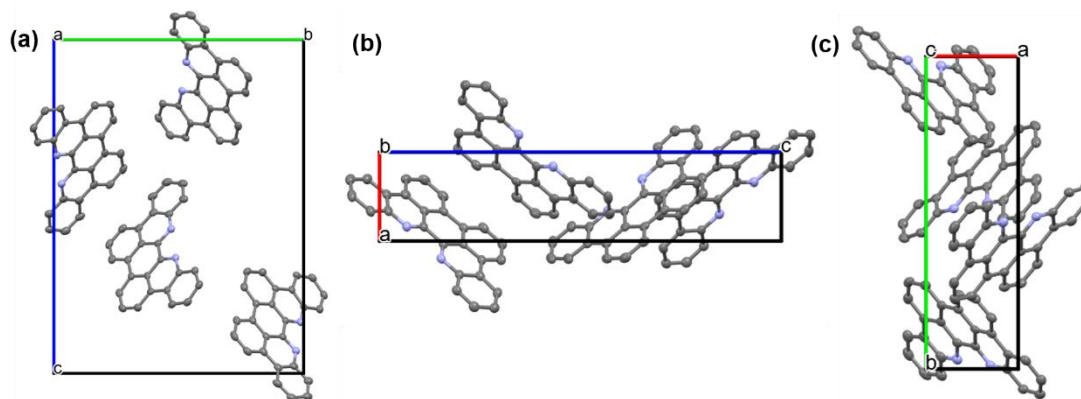


**Figure S9.** Packing diagram of **TB(phen)** in the single crystal of **[TB(phen)•C<sub>2</sub>H<sub>5</sub>OH]** along with (a) *a*; (b) *b*; (c) *c* cell axis.

**Section S3: Metal cation coordination study of TB(phen) in THF/CH<sub>3</sub>OH (1:1, v/v)**

**Uv-vis spectral studies**

*(1) General procedure for the Uv-vis spectral studies*

All Uv-vis spectra in this study were recorded using a Shimadzu UV-2600 spectrophotometer at 298 K. In all titration experiments, 2500  $\mu$ L of TB(phen) solution ( $2.00 \times 10^{-5}$  M or  $1.00 \times 10^{-5}$  M in THF/CH<sub>3</sub>OH (1:1, v/v)) was added to quartz cell. Each tested metal cation solution with a much higher concentration ( $1.00 \times 10^{-2}$  M or  $1.00 \times 10^{-3}$  M in THF/ CH<sub>3</sub>OH (1:1, v/v)) was then dropwise added. Data was collected after each aliquot was added and mixed. The concentration of TB(phen) was subject to slight dilution; this was accounted for mathematically using the Hyperquad Programme 2003.<sup>12</sup>

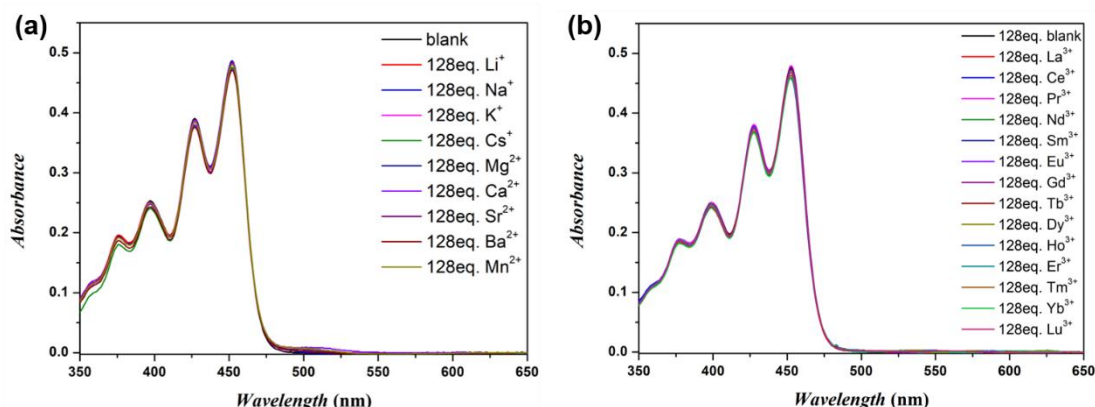
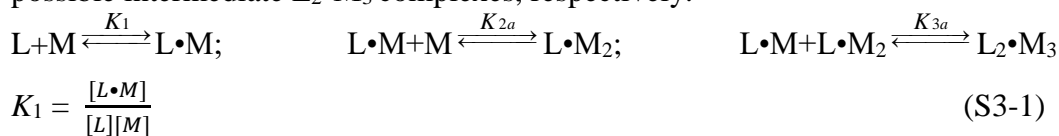


**Figure S10.** Uv-vis spectra of TB(phen) solution ( $2.00 \times 10^{-5}$  M in THF/ CH<sub>3</sub>OH (1:1, v/v)) in the absence 128 molar equiv of each tested alkali, alkaline earth, Mn<sup>2+</sup> or lanthanide metal cation.

The process of interaction between TB(phen) and metal cations involves multiple chemical equilibria, the relevant equilibria equations are given in the following:

1) This gave binding constants corresponding to the formation of L•M, L•M<sub>2</sub> and possible intermediate L<sub>2</sub>•M<sub>3</sub> complexes, respectively.



$$[L]_{all} = [L] + [L \cdot M] + [L \cdot M_2] + 2[L_2 \cdot M_3] \quad (S3-4)$$

$$[M]_{all} = [M] + [L \cdot M] + 2[L \cdot M_2] + 3[L_2 \cdot M_3] \quad (S3-5)$$

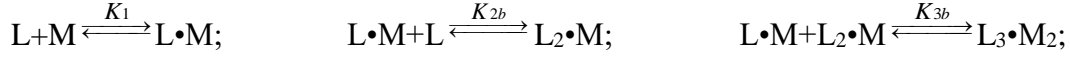
In Uv-vis spectroscopic titration process,

$$\begin{aligned} A &= A_{[L]} + A_{[L \cdot M]} + A_{[L \cdot M_2]} + A_{[L_2 \cdot M_3]} \\ &= \varepsilon_L [L]l + \varepsilon_{L \cdot M} [L \cdot M]l + \varepsilon_{L \cdot M_2} [L \cdot M_2]l + \varepsilon_{L_2 \cdot M_3} [L_2 \cdot M_3]l \end{aligned} \quad (S3-6)$$

In fluorescence spectroscopic titration process,

$$\begin{aligned} F &= F_{[L]} + F_{[L \cdot M]} + F_{[L \cdot M_2]} + F_{[L_2 \cdot M_3]} \\ &= k \phi_L [L] + k \phi_{L \cdot M} [L \cdot M] + k \phi_{L \cdot M_2} [L \cdot M_2] + k \phi_{L_2 \cdot M_3} [L_2 \cdot M_3] \end{aligned} \quad (S3-7)$$

2) This gave binding constants corresponding to the formation of  $L \cdot M$ ,  $L_2 \cdot M$  and possible intermediate  $L_3 \cdot M_2$  complexes, respectively.



$$K_1 = \frac{[L \cdot M]}{[L][M]}$$

$$K_{2b} = \frac{[L_2 \cdot M]}{[L \cdot M][L]} \quad (S3-8)$$

$$K_{3b} = \frac{[L_3 \cdot M_2]}{[L \cdot M][L_2 \cdot M]} \quad (S3-9)$$

$$[L]_{all} = [L] + [L \cdot M] + 2[L_2 \cdot M] + 3[L_3 \cdot M_2] \quad (S3-10)$$

$$[M]_{all} = [M] + [L \cdot M] + [L_2 \cdot M] + 2[L_3 \cdot M_2] \quad (S3-11)$$

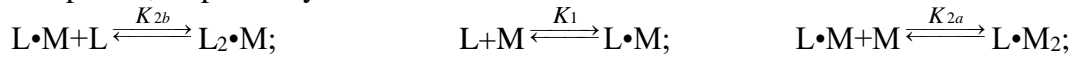
In Uv-vis spectroscopic titration process,

$$\begin{aligned} A &= A_{[L]} + A_{[L \cdot M]} + A_{[L_2 \cdot M]} + A_{[L_3 \cdot M_2]} \\ &= \varepsilon_L [L]l + \varepsilon_{L \cdot M} [L \cdot M]l + \varepsilon_{L_2 \cdot M} [L_2 \cdot M]l + \varepsilon_{L_3 \cdot M_2} [L_3 \cdot M_2]l \end{aligned} \quad (S3-12)$$

In fluorescence spectroscopic titration process,

$$\begin{aligned} F &= F_{[L]} + F_{[L \cdot M]} + F_{[L_2 \cdot M]} + F_{[L_3 \cdot M_2]} \\ &= k \phi_L [L] + k \phi_{L \cdot M} [L \cdot M] + k \phi_{L_2 \cdot M} [L_2 \cdot M] + k \phi_{L_3 \cdot M_2} [L_3 \cdot M_2] \end{aligned} \quad (S3-13)$$

3) This gave binding constants corresponding to the formation of  $L \cdot M$ ,  $L_2 \cdot M$  and  $L \cdot M_2$  complexes, respectively.



$$K_{2b} = \frac{[L_2 \cdot M]}{[L \cdot M][L]}$$

$$K_1 = \frac{[L \cdot M]}{[L][M]}$$

$$K_{2a} = \frac{[L \cdot M_2]}{[L \cdot M][M]}$$

$$[L]_{all} = [L] + [L \cdot M] + 2[L_2 \cdot M] + [L \cdot M_2] \quad (S3-14)$$

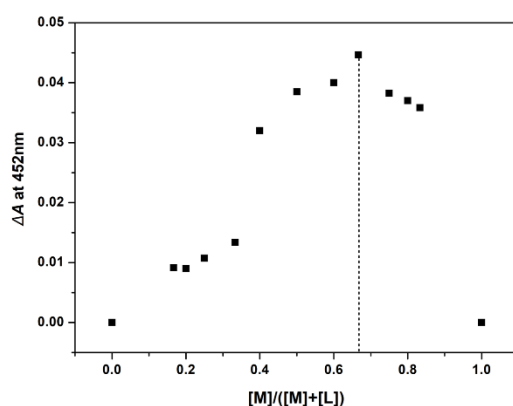
$$[M]_{all} = [M] + [L \cdot M] + [L_2 \cdot M] + 2[L \cdot M_2] \quad (S3-15)$$

In Uv-vis spectroscopic titration process,

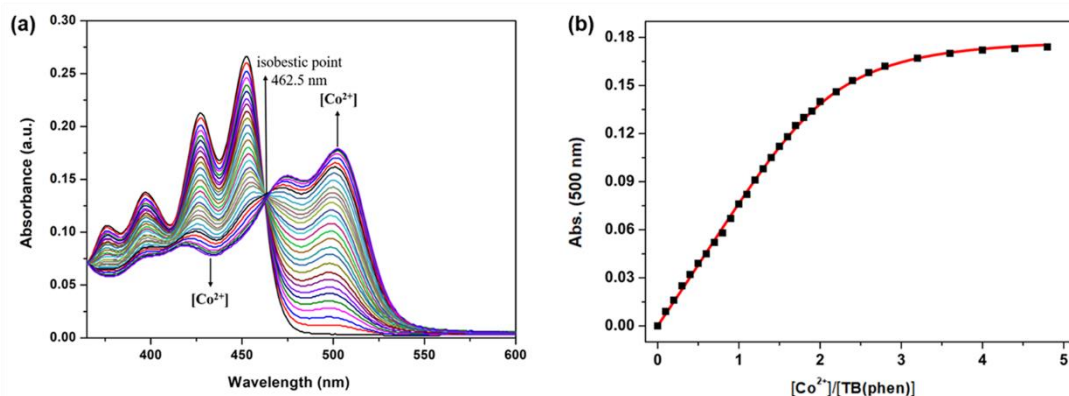
$$\begin{aligned} A &= A_{[L]} + A_{[L \cdot M]} + A_{[L_2 \cdot M]} + A_{[L \cdot M_2]} \\ &= \varepsilon_L [L] l + \varepsilon_{L \cdot M} [L \cdot M] l + \varepsilon_{L_2 \cdot M} [L_2 \cdot M] l + \varepsilon_{L \cdot M_2} [L \cdot M_2] l \end{aligned} \quad (S3-16)$$

In fluorescence spectroscopic titration process,

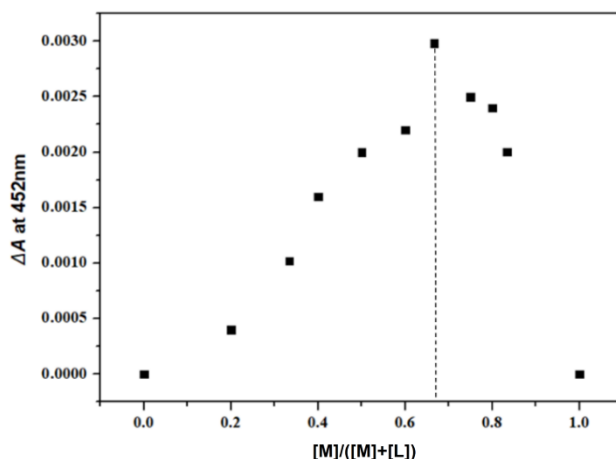
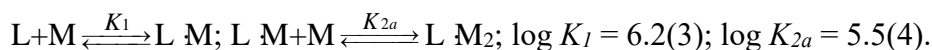
$$\begin{aligned} F &= F_{[L]} + F_{[L \cdot M]} + F_{[L_2 \cdot M]} + F_{[L \cdot M_2]} \\ &= k \phi_L [L] + k \phi_{L \cdot M} [L \cdot M] + k \phi_{L_2 \cdot M} [L_2 \cdot M] + k \phi_{L \cdot M_2} [L \cdot M_2] \end{aligned} \quad (S3-17)$$



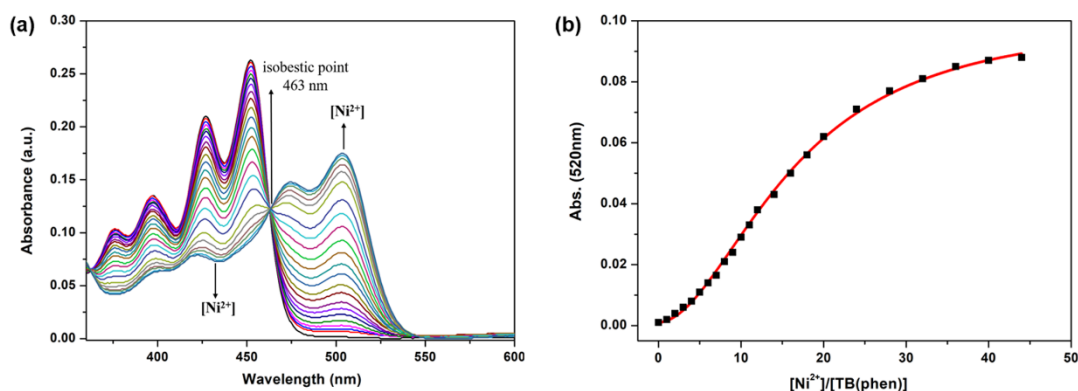
**Figure S11.** Job plot corresponding to the interactions between **TB(phen)** and  $\text{Co}^{2+}$  in THF/ $\text{CH}_3\text{OH}$  (1:1,  $v/v$ ) at 298 K as monitored via Uv-vis spectroscopy.  $[\text{Ligand}] + [\text{Metal}] = 0.040$  mM. Maximum value was seen at 0.667 in the case of  $\text{Co}^{2+}$ , this supports the 1:2 (ligand/metal) stoichiometry as suggested in the main text.



**Figure S12.** (a) Uv-vis spectra recorded for a solution of **TB(phen)** ( $1.00 \times 10^{-5}$  M in THF/MeOH (1:1,  $v/v$ )) as a function of increasing  $\text{Co}^{2+}$  concentration (from 0 to 4.8 molar equiv) at 298 K. (b) The change in the absorbance at 500 nm (“■”) and the results of the corresponding nonlinear curve fitting according calculated model (red line) using Hyperquad 2003.<sup>12</sup> The equilibriums and related  $K_a$  calculation results as shown:

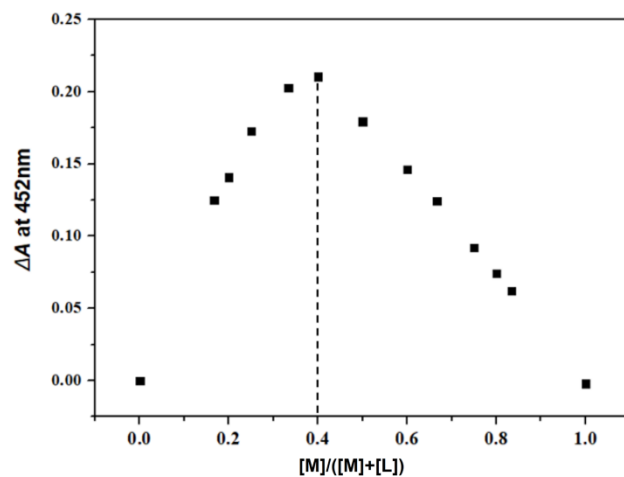


**Figure S13.** Job plot corresponding to the interactions between **TB(phen)** and  $Ni^{2+}$  in THF/ $CH_3OH$  (1:1, v/v) at 298 K as monitored via Uv-vis spectroscopy. [Ligand] + [Metal] = 0.040 mM. Maximum value was seen at 0.667 in the case of  $Ni^{2+}$ , this supports the 1:2 (ligand/metal) stoichiometry as suggested in the main text.

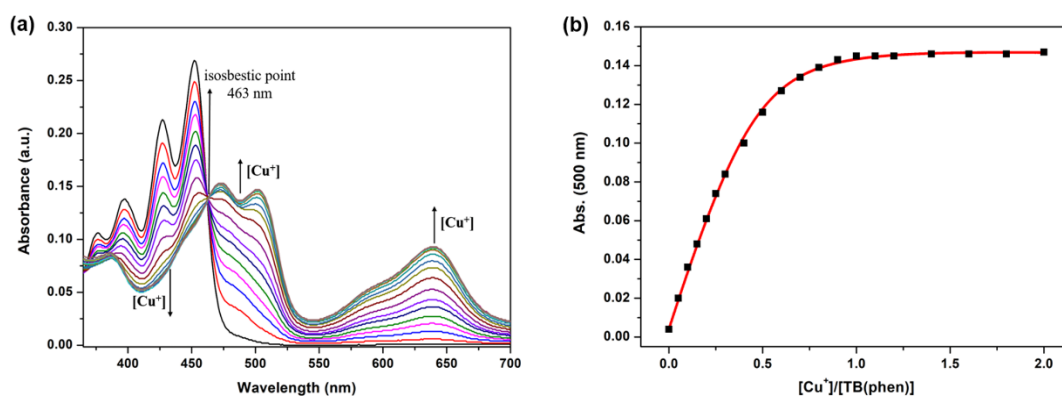


**Figure S14.** (a) Uv-vis spectra recorded for a solution of **TB(phen)** ( $1.00 \times 10^{-5}$  M in THF/ $CH_3OH$  (1:1, v/v)) as a function of increasing  $Ni^{2+}$  concentration (from 0 to 42 molar equiv) at 298 K. (b) The change in the absorbance at 520 nm (“■”) and the results of the corresponding nonlinear curve fitting according calculated model (red line) using Hyperquad 2003.<sup>12</sup> The equilibriums and related  $K_a$  calculation results as shown:



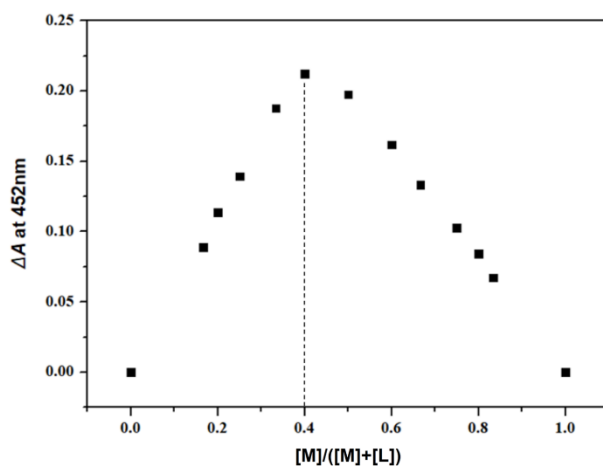


**Figure S15.** Job plot corresponding to the interactions between **TB(phen)** and  $\text{Cu}^+$  in THF/ $\text{CH}_3\text{OH}$  (1:1,  $v/v$ ) at 298 K as monitored via Uv-vis spectroscopy.  $[\text{Ligand}] + [\text{Metal}] = 0.040 \text{ mM}$ . Maximum value was seen at 0.4 in the case of  $\text{Cu}^+$ , this supports the 2:1 and 1:1 (ligand/metal) stoichiometry as suggested in the main text.

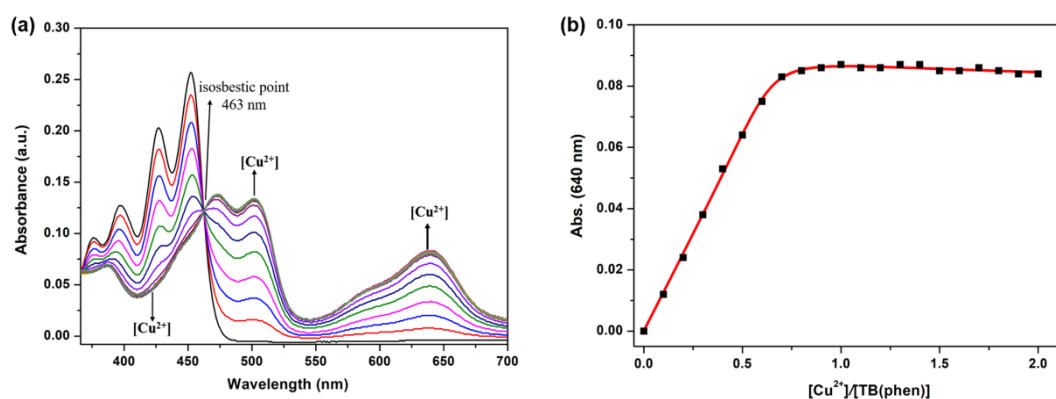


**Figure S16.** (a) Uv-vis spectra recorded for a solution of **TB(phen)** ( $1.00 \times 10^{-5} \text{ M}$  in THF/ $\text{CH}_3\text{OH}$  (1:1,  $v/v$ )) as a function of increasing  $\text{Cu}^+$  concentration (from 0 to 2.0 molar equiv) at 298 K. (b) The change in the absorbance at 500 nm (“■”) and the results of the corresponding nonlinear curve fitting according calculated model (red line) using Hyperquad 2003.<sup>12</sup> The equilibriums and related  $K_a$  calculation results as shown:

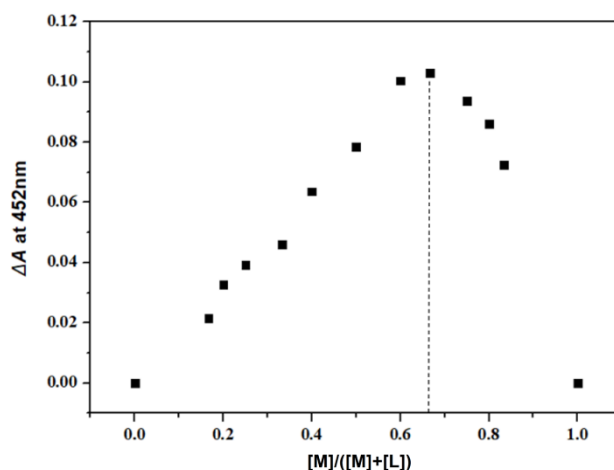




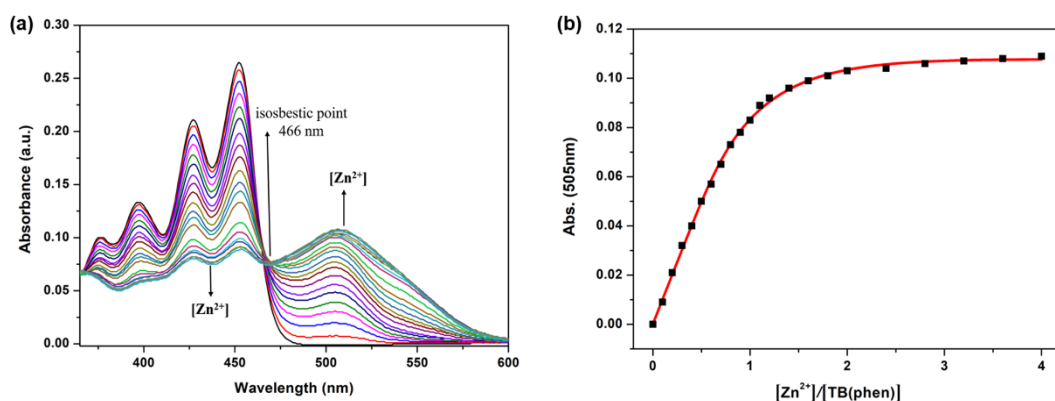
**Figure S17.** Job plot corresponding to the interactions between **TB(phen)** and  $\text{Cu}^{2+}$  in THF/ $\text{CH}_3\text{OH}$  (1:1,  $v/v$ ) at 298 K as monitored via Uv-vis spectroscopy. [Ligand] + [Metal] = 0.040 mM. Maximum value was seen at 0.4 in the case of  $\text{Cu}^{2+}$ , this supports the 2:1 and 1:1 (ligand/metal) stoichiometry as suggested in the main text.



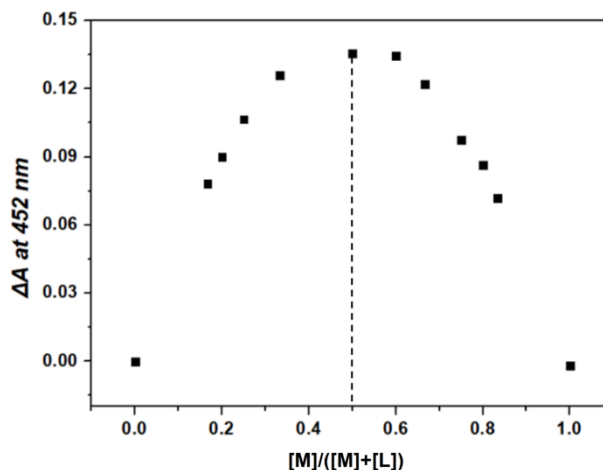
**Figure S18.** (a) Uv-vis spectra recorded for a solution of **TB(phen)** ( $1.00 \times 10^{-5}$  M in THF/MeOH (1:1,  $v/v$ )) as a function of increasing  $\text{Cu}^{2+}$  concentration (from 0 to 2.0 molar equiv) at 298 K. (b) The change in the absorbance at 640 nm (“■”) and the results of the corresponding nonlinear curve fitting according calculated model (red line) using Hyperquad 2003.<sup>12</sup> The equilibriums and related  $K_a$  calculation results as shown:  
 $\text{L} + \text{M} \xrightleftharpoons{K_1} \text{L M}$ ;  $\text{L M} + \text{L} \xrightleftharpoons{K_{2b}} \text{L}_2 \text{ M}$ ;  $\text{L M} + \text{L}_2 \text{ M} \xrightleftharpoons{K_{3b}} \text{L}_3 \text{ M}_2$ ;  $\log K_1 = 6.6(3)$ ;  $\log K_{2b} = 5.9(6)$ ;  $\log K_{3b} = 6.1(5)$ .



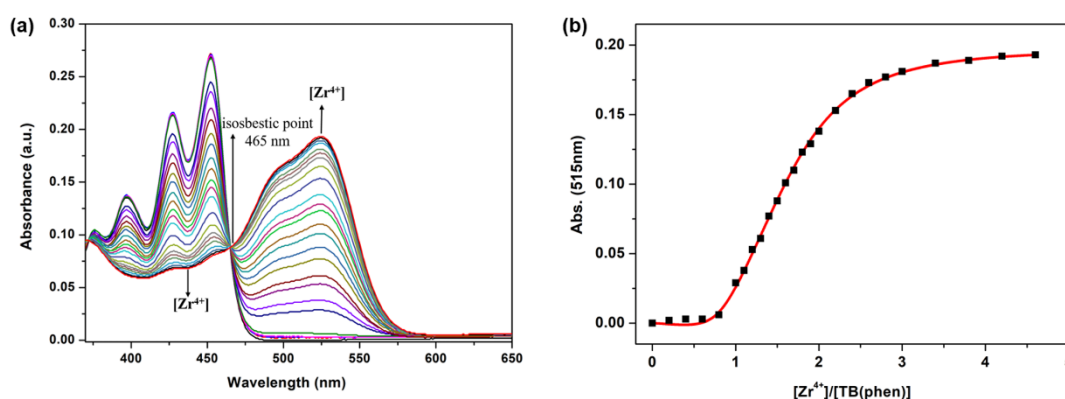
**Figure S19.** Job plot corresponding to the interactions between **TB(phen)** and  $\text{Zn}^{2+}$  in THF/ $\text{CH}_3\text{OH}$  (1:1,  $v/v$ ) at 298 K as monitored via Uv-vis spectroscopy.  $[\text{Ligand}] + [\text{Metal}] = 0.040$  mM. Maximum value was seen at 0.667 in the case of  $\text{Zn}^{2+}$ , this supports the 1:2 (ligand/metal) stoichiometry as suggested in the main text.



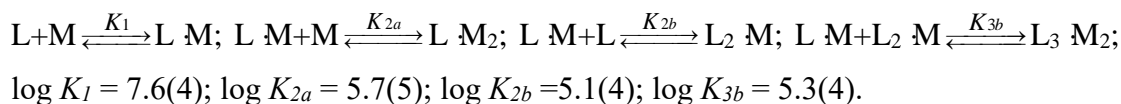
**Figure S20.** (a) Uv-vis spectra recorded for a solution of **TB(phen)** ( $1.00 \times 10^{-5}$  M in THF/ $\text{CH}_3\text{OH}$  (1:1,  $v/v$ )) as a function of increasing  $\text{Zn}^{2+}$  concentration (from 0 to 4.0 molar equiv) at 298 K. (b) The change in the absorbance at 505 nm (“■”) and the results of the corresponding nonlinear curve fitting according calculated model (red line) using Hyperquad 2003.<sup>12</sup> The equilibriums and related  $K_a$  calculation results as shown:  
 $\text{L} + \text{M} \xrightleftharpoons{K_1} \text{L M}$ ;  $\text{L M} + \text{M} \xrightleftharpoons{K_{2a}} \text{L M}_2$ ;  $\text{L M} + \text{L} \xrightleftharpoons{K_{2b}} \text{L}_2 \text{ M}$ ;  $\log K_1 = 6.9(3)$ ;  $\log K_{a2} = 5.1(4)$ ;  $\log K_{a4} = 5.6(5)$ .



**Figure S21.** Job plot corresponding to the interactions between **TB(phen)** and  $Zr^{4+}$  in THF/ $CH_3OH$  (1:1,  $v/v$ ) at 298 K as monitored via Uv-vis spectroscopy. [Ligand] + [Metal] = 0.040 mM. Maximum value was seen at 0.5 in the case of  $Zr^{4+}$ , this supports the 1:1 (ligand/metal) stoichiometry as suggested in the main text.



**Figure S22.** (a) Uv-vis spectra recorded for a solution of **TB(phen)** ( $1.00 \times 10^{-5}$  M in THF/ $CH_3OH$  (1:1,  $v/v$ )) as a function of increasing  $Zr^{4+}$  concentration (from 0 to 4.6 molar equiv) at 298 K. (b) The change in the absorbance at 515 nm (“■”) and the results of the corresponding nonlinear curve fitting according calculated model (red line) using Hyperquad 2003.<sup>12</sup> The equilibriums and related  $K_a$  calculation results as shown:



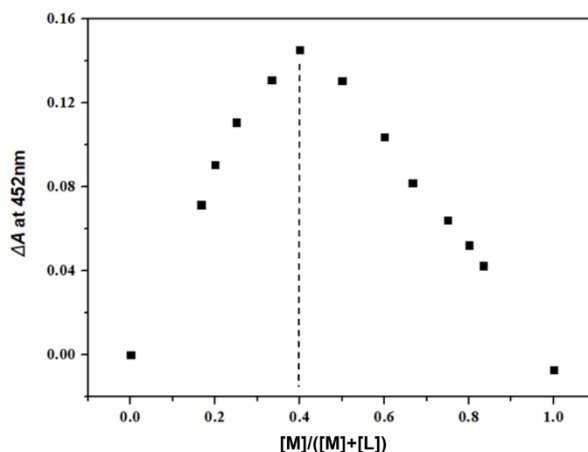


**Figure S23.** Job plot corresponding to the interactions between **TB(phen)** and  $\text{Ag}^+$  in THF/ $\text{CH}_3\text{OH}$  (1:1,  $v/v$ ) at 298 K as monitored via Uv-vis spectroscopy. [Ligand] + [Metal] = 0.040 mM. Maximum value was seen at 0.4 in the case of  $\text{Ag}^+$ , this supports the 2:1 and 1:1(ligand/metal) stoichiometry as suggested in the main text.

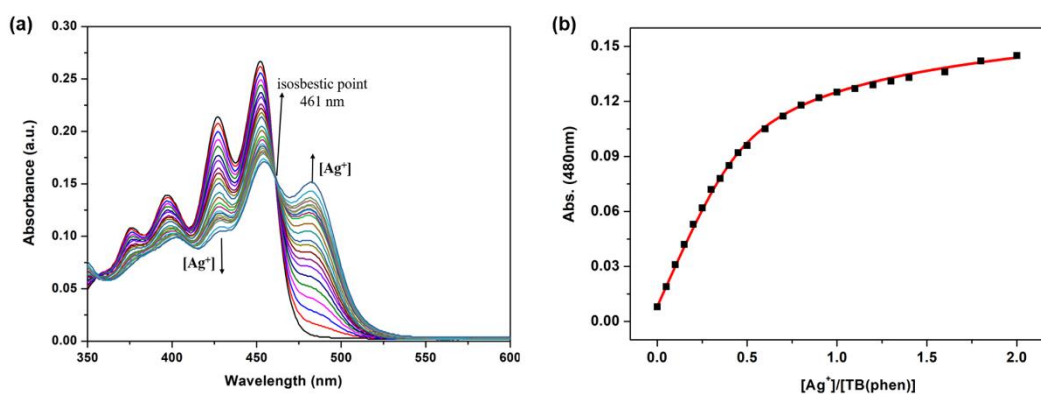


**Figure S24.** (a) Uv-vis spectra recorded for a solution of **TB(phen)** ( $1.00 \times 10^{-5}$  M in THF/MeOH (1:1,  $v/v$ )) as a function of increasing  $\text{Ag}^+$  concentration (from 0 to 2.0 molar equiv) at 298 K. (b) The change in the absorbance at 480 nm (“■”) and the results of the corresponding nonlinear curve fitting according calculated model (red line) using Hyperquad 2003.<sup>12</sup> The equilibriums and related  $K_a$  calculation results as shown:  
 $\text{L} + \text{M} \xrightleftharpoons{K_1} \text{L} \cdot \text{M}$ ;  $\text{L} \cdot \text{M} + \text{L} \xrightleftharpoons{K_{2b}} \text{L}_2 \cdot \text{M}$ ;  $\log K_1 = 5.4(3)$ ;  $\log K_{2b} = 6.2(5)$ .

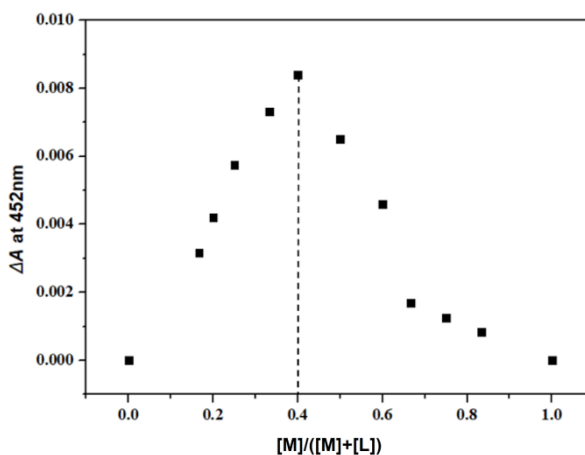


**Figure S25.** Job plot corresponding to the interactions between **TB(phen)** and  $\text{Cd}^{2+}$  in THF/ $\text{CH}_3\text{OH}$  (1:1, v/v) at 298 K as monitored via Uv-vis spectroscopy. [Ligand] + [Metal] = 0.040 mM. Maximum value was seen at 0.4 in the case of  $\text{Cd}^{2+}$ , this supports the 2:1 and 1:1 (ligand/metal) stoichiometry as suggested in the main text.

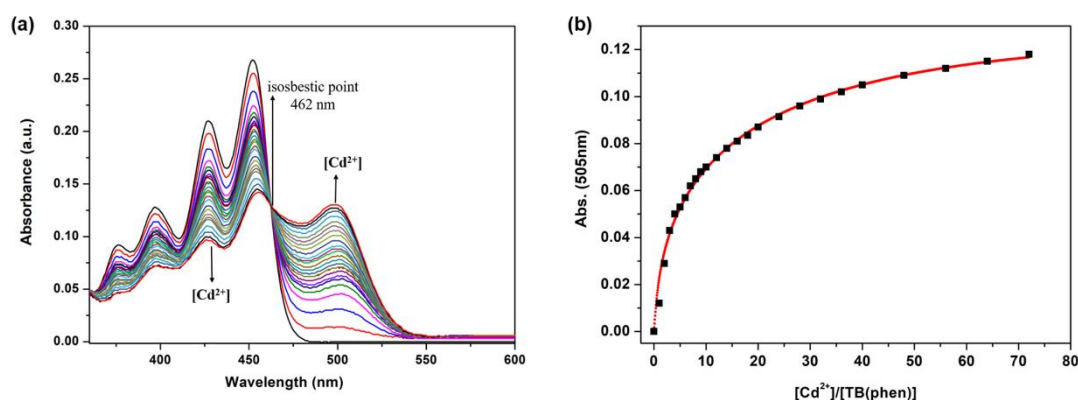


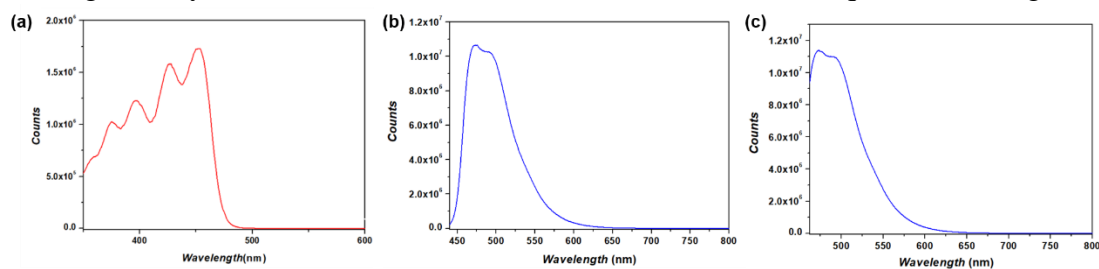
**Figure S26.** (a) Uv-vis spectra recorded for a solution of **TB(phen)** ( $1.00 \times 10^{-5}$  M) in THF/ $\text{CH}_3\text{OH}$  (1:1, v/v) as a function of increasing  $\text{Cd}^{2+}$  concentration (from 0 to 72 molar equiv) at 298 K. (b) The change in the absorbance at 500 nm (“■”) and the results of the corresponding nonlinear curve fitting according calculated model (red line) using Hyperquad 2003.<sup>10</sup> The equilibriums and related  $K_a$  calculation results as shown:



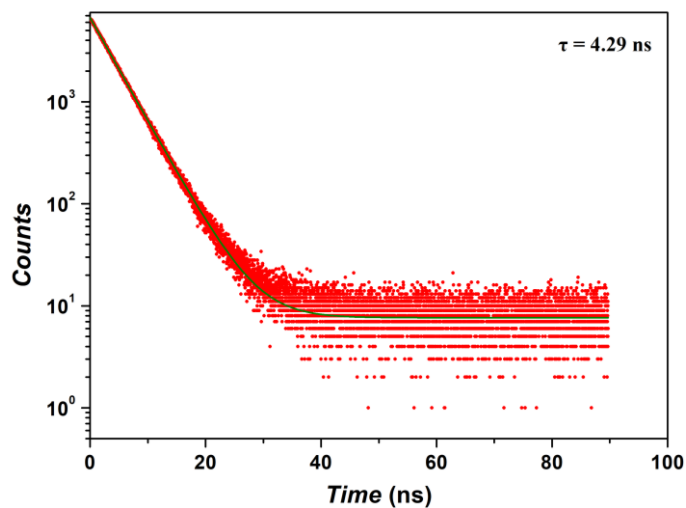
### Fluorescence spectroscopic studies

Fluorescence spectra were recorded using an Edinburgh Instruments FS5 spectrometer. A 2500  $\mu\text{L}$  solution of **TB(phen)** ( $1.00 \times 10^{-5}$  M in THF/ $\text{CH}_3\text{OH}$  (1:1, v/v)) was added to a sample cell. Specific metal ions solutions at much higher concentrations ( $1.00 \times 10^{-2}$  M or  $1.00 \times 10^{-3}$  M in THF/ $\text{CH}_3\text{OH}$  (1:1, v/v)) were then

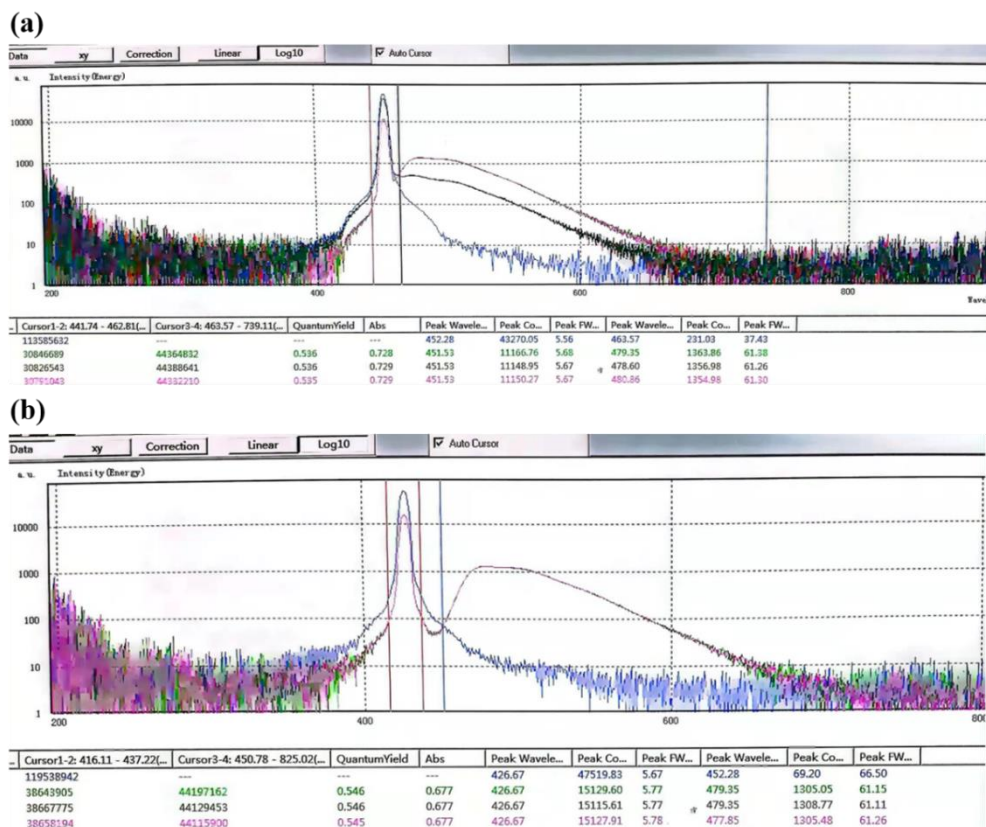
added gradually. Data was collected after each addition and subsequent to mixing.



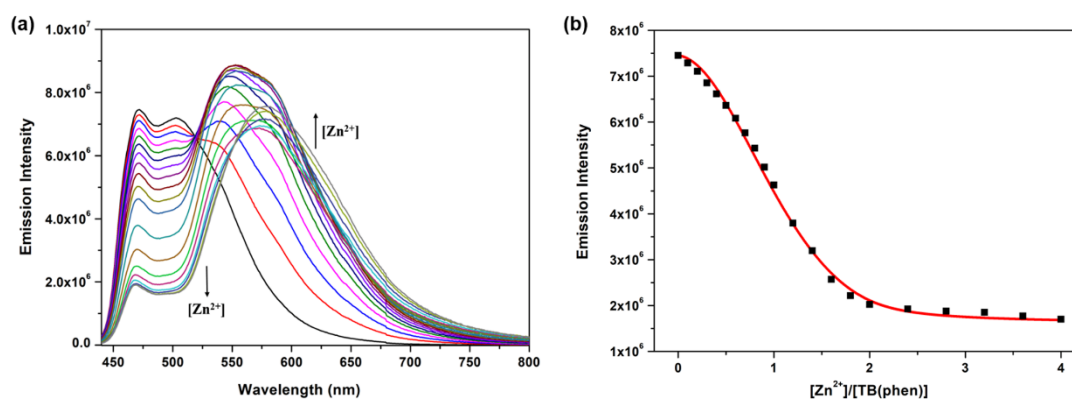
**Figure S27.** (a) Excitation spectrum of **TB(phen)** solution ( $1.00 \times 10^{-5}$  M in THF/CH<sub>3</sub>OH (1:1, v/v),  $\lambda_{em} = 490$  nm). (b) Emission spectrum of **TB(phen)** solution ( $1.00 \times 10^{-5}$  M in THF/CH<sub>3</sub>OH (1:1, v/v)),  $\lambda_{ex} = 427$  nm. (c) Emission spectrum of **TB(phen)** solution ( $1.00 \times 10^{-5}$  M in THF/CH<sub>3</sub>OH (1:1, v/v)),  $\lambda_{ex} = 450$  nm (Voltage = 400 V, entrance slit width = 5 nm, exit slit width = 8 nm).



**Figure S28.** The fluorescence lifetime of **TB(phen)** solution ( $1.00 \times 10^{-5}$  M in THF/CH<sub>3</sub>OH (1:1, v/v) at excitation wavelength of 450 nm.

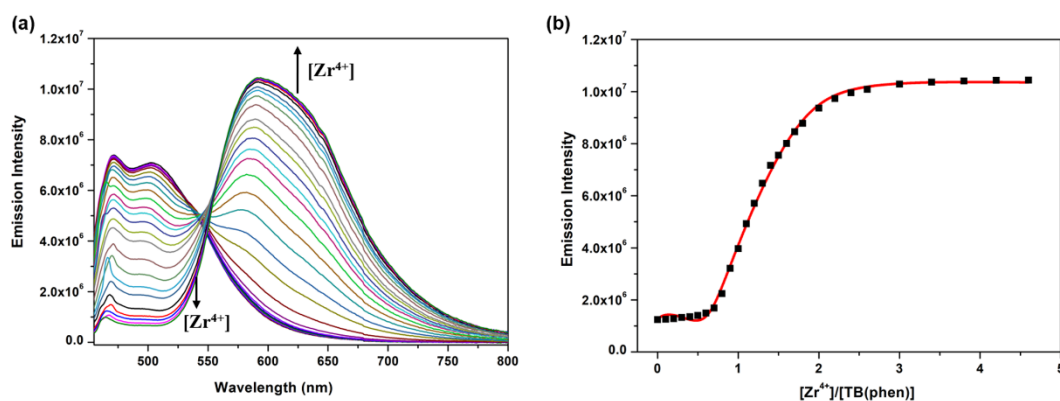


**Figure S29.** The fluorescence quantum yield of **TB(phen)** solution ( $1.00 \times 10^{-5}$  M in THF/CH<sub>3</sub>OH (1:1, v/v) at excitation wavelength of 452 nm (a) and 427 nm (b).

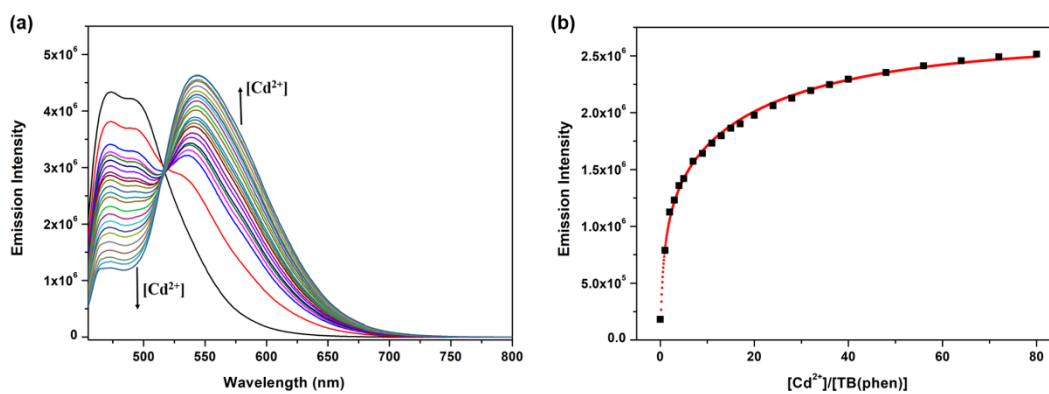
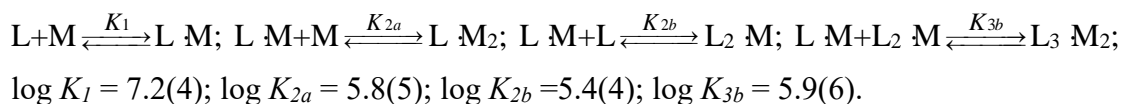


**Figure S30.** (a) Fluorescent emission spectra a solution of **TB(phen)** ( $1.00 \times 10^{-5}$  M in THF/CH<sub>3</sub>OH (1:1, v/v) with increasing Zn<sup>2+</sup> concentration (from 0 to 4.0 molar equiv) at 298 K. ( $\lambda_{ex} = 466$  nm, voltage = 400 V, entrance slit width = 5 nm, exit slit width = 8 nm) (b) The change in the fluorescence intensity at 500 nm (“■”) and the corresponding simulated emission intensity (red line). The equilibriums and related  $K_a$  calculations result as shown:

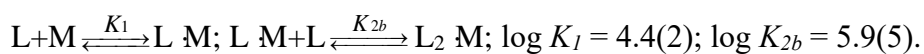




**Figure S31.** (a) Fluorescent emission spectra a solution of **TB(phen)** ( $1.00 \times 10^{-5}$  M in THF/CH<sub>3</sub>OH (1:1, v/v)) with increasing Zr<sup>4+</sup> concentration (from 0 to 4.6 molar equiv) at 298 K. ( $\lambda_{\text{ex}} = 465$  nm, Voltage = 400 V, entrance slit width = 5 nm, exit slit width = 8 nm) (b) change in the fluorescence intensity at 600 nm (“■”) and the corresponding simulated emission intensity (red line). The equilibriums and related  $K_a$  calculation results as shown:



**Figure S32.** (a) Fluorescent emission spectra a solution of **TB(phen)** ( $1.00 \times 10^{-5}$  M in THF/CH<sub>3</sub>OH (1:1, v/v)) with increasing Cd<sup>2+</sup> concentration (from 0 to 80 molar equiv) at 298 K. ( $\lambda_{\text{ex}} = 462$  nm, Voltage = 400 V, entrance slit width = 5 nm, exit slit width = 8 nm) (b) The change in the fluorescence intensity at 560 nm (“■”) and the corresponding simulated emission intensity (red line). The equilibriums and related  $K_a$  calculation results as shown:



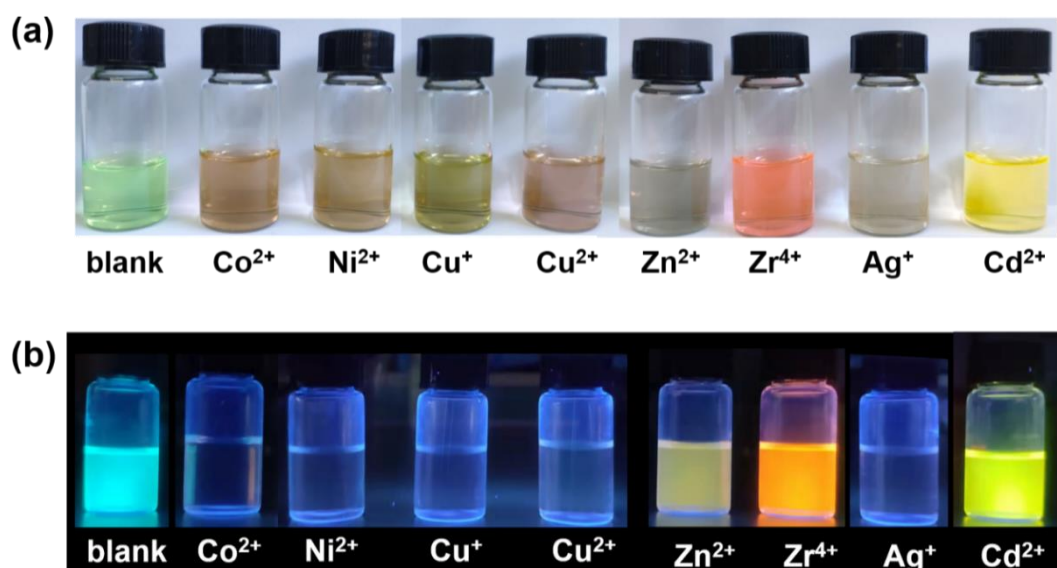


**Figure S33.** Photographs of **TB(phen)** solution ( $2.00 \times 10^{-5}$  M) coordination with transition metal cations in THF/CH<sub>3</sub>OH (1:1, v/v) under visible light and 365 nm UV light, respectively.

**Mass spectroscopic studies of the complexes formed between TB(phen) (L) and metal cations.**

Adding 10 molar equiv of metal cations into **TB(phen)** solution in THF/CH<sub>3</sub>OH (1:1, v/v). The mixture solution was subjected to electrospray high resolution mass spectra (ESI-HRMS) analysis via infusion using a Bruker Solarix XR FTMS operating in the positive ion model. Several ions ascribable a ligand/metal complexes were seen in the gas phase as presented below.

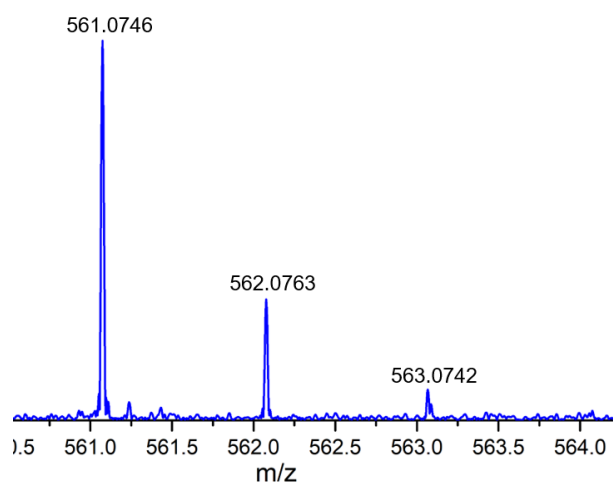


**Figure 34.** ESI high resolution mass spectrum of **L•Co<sup>2+</sup>**, Calcd. for **[L+Co<sup>2+</sup>+2NO<sub>3</sub><sup>-</sup>+H<sub>2</sub>O+6H]<sup>+</sup>** 561.0819, found 561.0746.

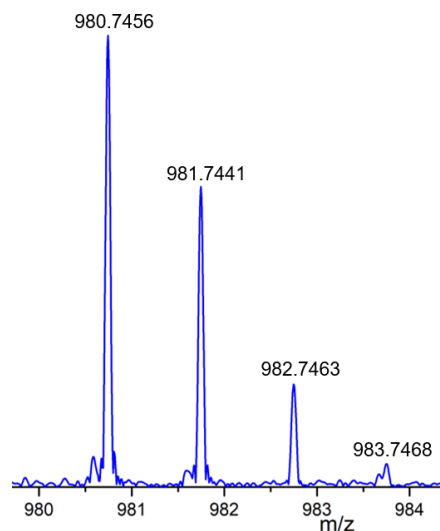


**Figure 35.** ESI high resolution mass spectrum of  $L \cdot 2Co^{2+}$ , Calcd. for  $[L+2Co^{2+}+4NO_3^-+5K+4H_2O-6H]^+$  980.7474, found 980.7456.

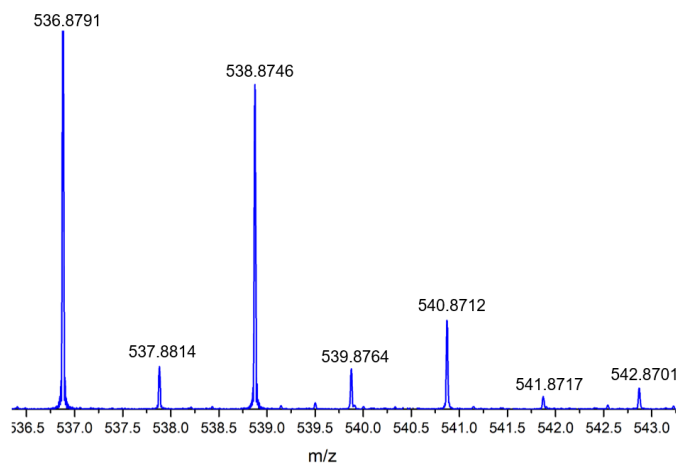


**Figure 36.** ESI high resolution mass spectrum of  $L \cdot Ni^{2+}$ , Calcd. for  $[L+Ni^{2+}+2Cl^-+K+Na-7H]^+$  536.8877, found 536.8791.

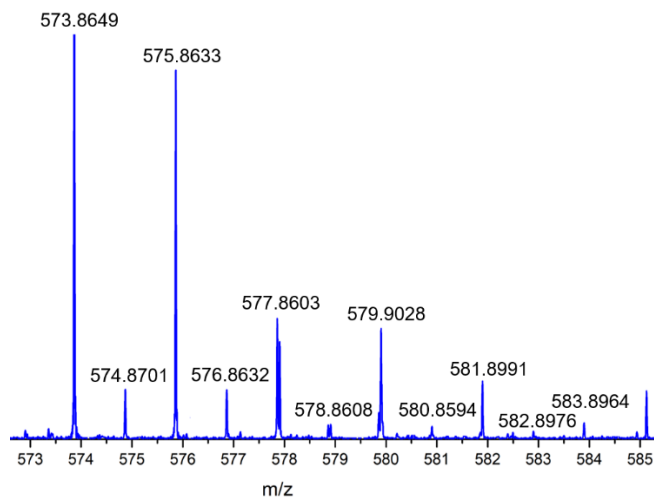


**Figure 37.** ESI high resolution mass spectrum of  $L \cdot 2Ni^{2+}$ , Calcd. for  $[L+2Ni^{2+}+3Cl^-+H]^+$  573.8853, found 573.8649.

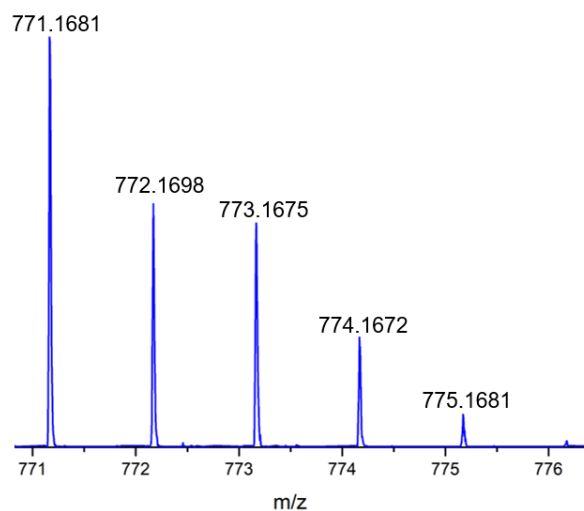


**Figure 38.** ESI high resolution mass spectrum of  $L_2 \cdot Cu^{2+}$ , Calcd. for  $[2L + Cu^{2+}]^{+}$  771.1610, found 771.1681.

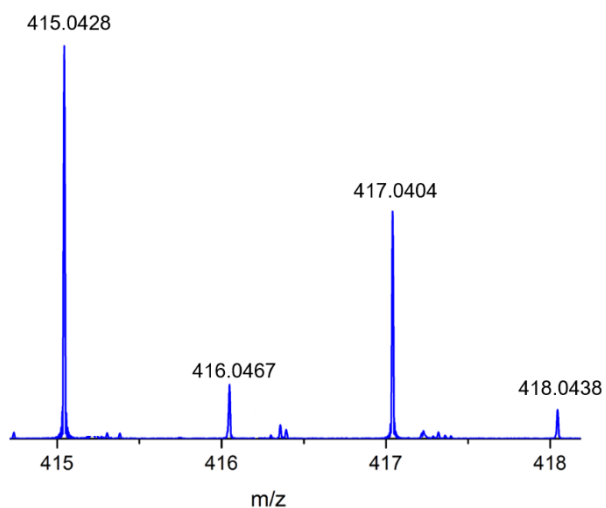


**Figure 39.** ESI high resolution mass spectrum of  $L \cdot Cu^{2+}$ , Calcd. for  $[L + Cu^{2+} - 2H]^{+}$  415.0297, found 415.0428.

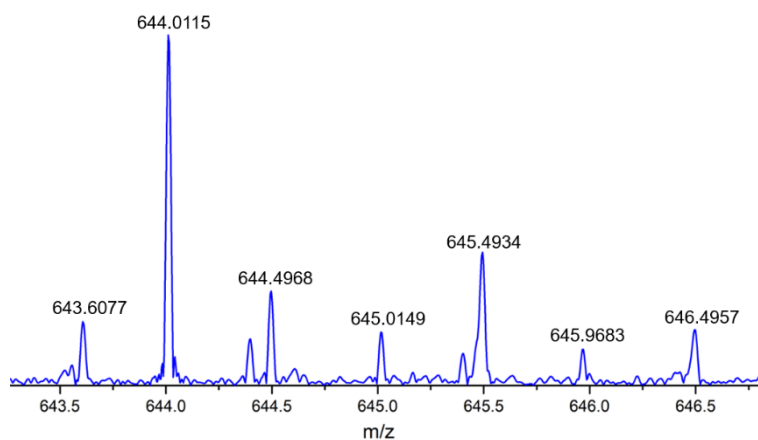


**Figure 40.** ESI high resolution mass spectrum of  $L_3 \cdot 2Cu^{2+}$ , Calcd. for  $[3L + 2Cu^{2+} + K + 3Na - 8H]^{2+}$  644.0385, found 644.0115.

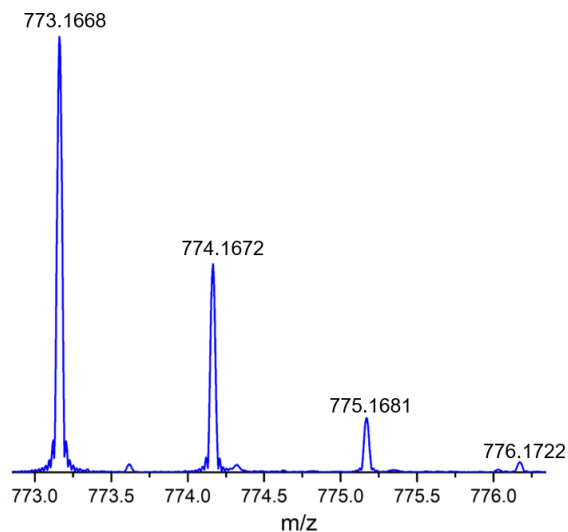


**Figure 41.** ESI high resolution mass spectrum of  $L_2 \cdot Zn^{2+}$ , Calcd. for  $[2L+Zn^{2+}+H]^+$  773.1683, found 733.1668.

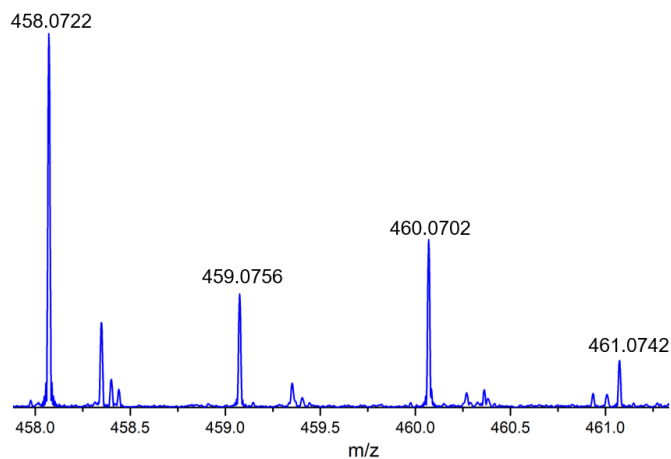


**Figure 42.** ESI high resolution mass spectrum of  $L \cdot Zn^{2+}$ , Calcd. for  $[L+Zn^{2+}+2H_2O+4H]^+$  458.0972, found 458.0722.

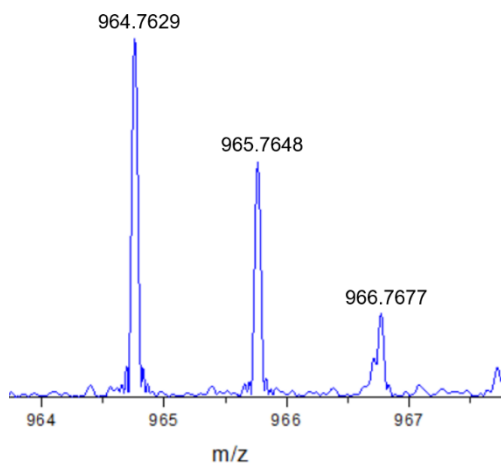


**Figure 43.** ESI high resolution mass spectrum of  $L \cdot 2Zn^{2+}$ , Calcd. for  $[L+2Zn^{2+}+4NO_3^-+4K+2Na+2H_2O-3H]^+$  964.7574, found 964.7629.

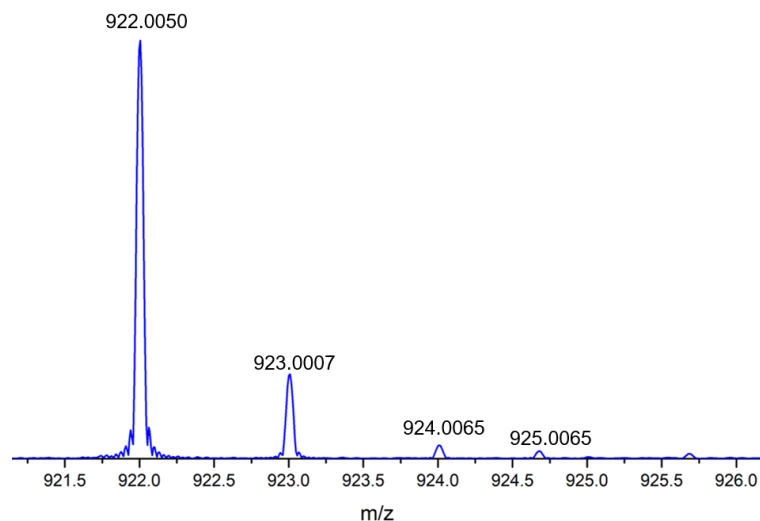


**Figure 44.** ESI high resolution mass spectrum of  $L_2 \cdot Zr^{4+}$ , Calcd. for  $[2L + Zr^{4+} + 3Cl + Na - 4H]^+$  922.0014, found 922.0050.

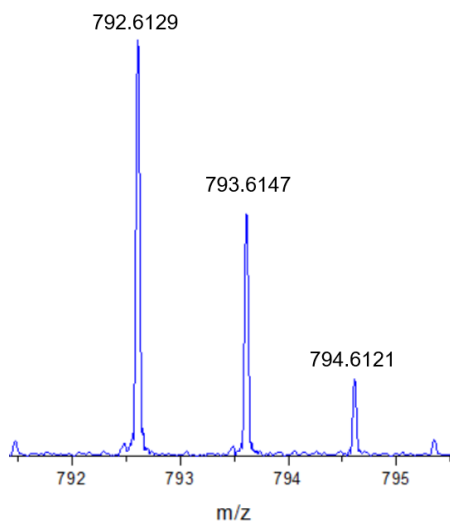


**Figure 45.** ESI high resolution mass spectrum of  $L \cdot Zr^{4+}$ , Calcd. for  $[L + Zr^{4+} + 4Cl + 5K + Na - 9H]^+$  792.6341, found 792.6129.

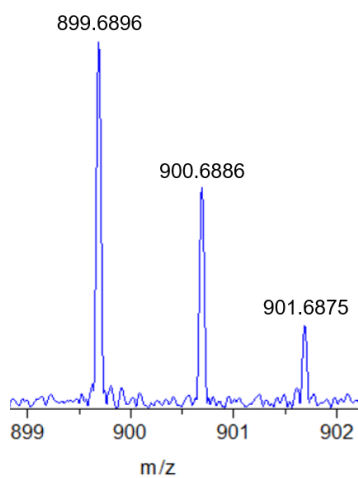


**Figure 46.** ESI high resolution mass spectrum of  $L \cdot 2Zr^{4+}$ , Calcd. for  $[L + 2Zr^{4+} + 8Cl + K + Na + H_2O + 6H]^+$  899.6872, found 899.6896.

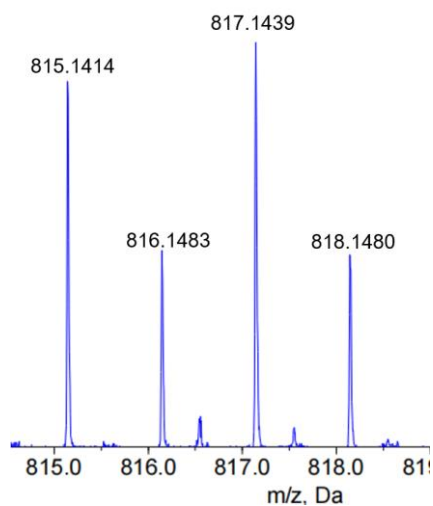


**Figure 47.** ESI high resolution mass spectrum of  $L_2 \cdot Ag^+$ , Calcd. for  $[2L+Ag^+]^+$  815.1365, found 815.1414.

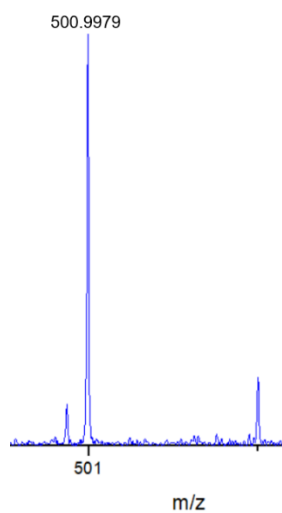


**Figure 48.** ESI high resolution mass spectrum of  $L \cdot Ag^+$ , Calcd. for  $[L+Ag^+K+H]^+$  500.9923, found 500.9979.

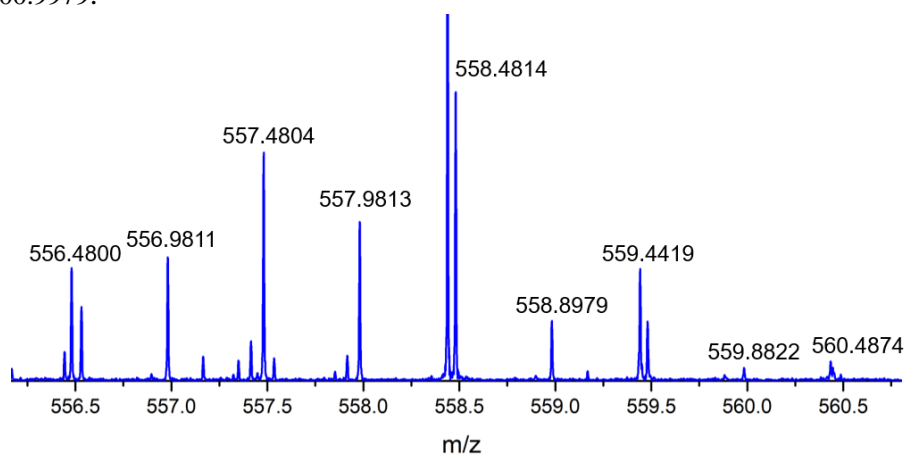


**Figure 49.** ESI high resolution mass spectrum of  $L_2 \cdot Cd^+$ , Calcd. for  $[2L+Cd^{2+}+2NO_3^-+4K+H_2O-3H]^2+$  558.4762, found 558.4814.

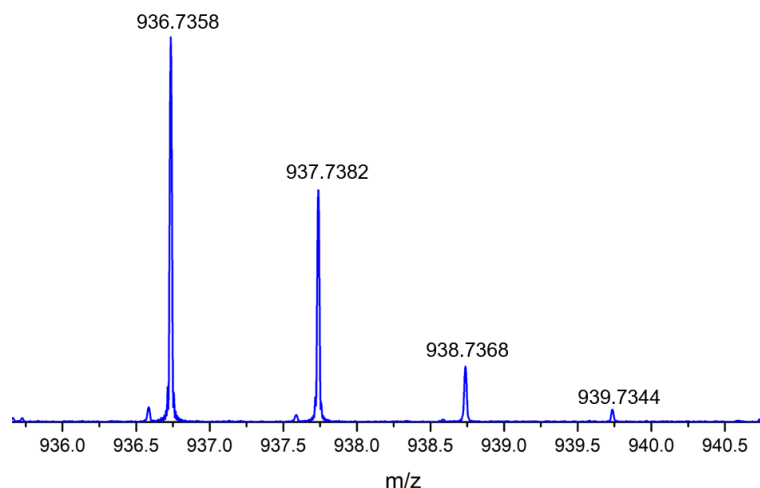


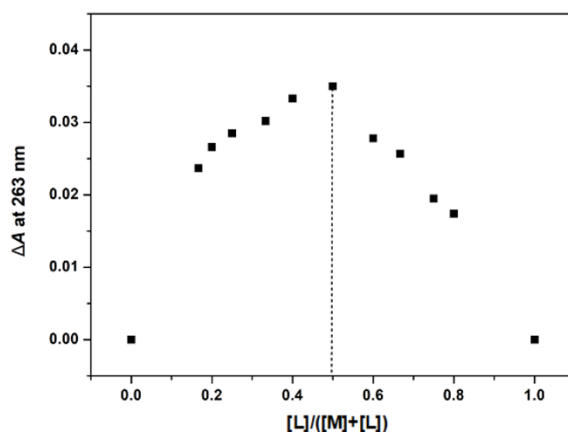
**Figure 50.** ESI high resolution mass spectrum of  $L\cdot Cd^{2+}$ , Calcd. for  $[L+Cd^{2+}+2NO_3^-+7K+3Na+3H]^+$  936.7334, found 936.7358.

**Table S2.** Summary of ESI-HRMS results

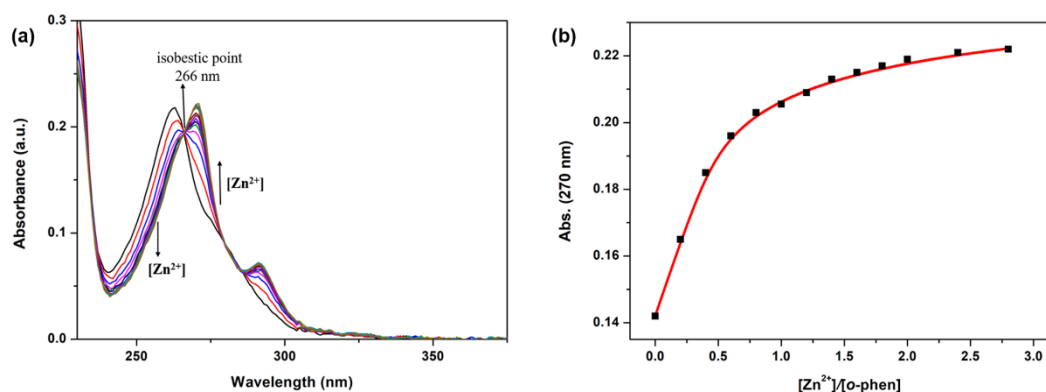
Presumed Complex	Peak Assignment	Calculated m/z	Observed m/z value
$[L\cdot Co^{2+}]$	$[L+Co^{2+}+2NO_3^-+H_2O+6H]^{++}$	561.0819	561.0746
$[L\cdot 2Co^{2+}]$	$[L+2Co^{2+}+4NO_3^-+5K+4H_2O-6H]^{++}$	980.7474	980.7456
$[L\cdot Ni^{2+}]$	$[L+Ni^{2+}+2Cl^-+K+Na-7H]^{++}$	536.8877	536.8791
$[L\cdot 2Ni^{2+}]$	$[L+2Ni^{2+}+3Cl^-+H]^{++}$	573.8853	573.8649
$[L_2\cdot Cu^{2+}]$	$[2L+Cu^{2+}]^{++}$	771.1610	771.1681
$[L\cdot Cu^{2+}]$	$[L+Cu^{2+}-2H]^{++}$	415.0297	415.0428
$[L_3\cdot 2Cu^{2+}]$	$[3L+2Cu^{2+}+K+3Na-8H]^{2++}$	644.0385	644.0115
$[L_2\cdot Zn^{2+}]$	$[2L+Zn^{2+}+H]^{++}$	773.1683	773.1668
$[L\cdot Zn^{2+}]$	$[L+Zn^{2+}+2H_2O+4H]^{++}$	458.0972	458.0722
$[L\cdot 2Zn^{2+}]$	$[L+2Zn^{2+}+4NO_3^-+4K+2Na+2H_2O-3H]^{++}$	964.7574	964.7629
$[L_2\cdot Zr^{4+}]$	$[2L+Zr^{4+}+3Cl^-+Na-4H]^{++}$	922.0014	922.0050
$[L\cdot Zr^{4+}]$	$[L+Zr^{4+}+4Cl^-+5K+Na-9H]^{++}$	792.6341	792.6129
$[L\cdot 2Zr^{4+}]$	$[L+2Zr^{4+}+8Cl^-+K+Na+H_2O-6H]^{++}$	899.6872	899.6896
$[L_2\cdot Ag^+]$	$[2L+Ag^+]^{++}$	815.1365	815.1414
$[L\cdot Ag^+]$	$[L+Ag^++K+H]^{++}$	500.9923	500.9979
$[L_2\cdot Cd^{2+}]$	$[2L+Cd^{2+}+2NO_3^-+4K+H_2O-3H]^{2++}$	558.4762	558.4801
$[L\cdot Cd^{2+}]$	$[L+Cd^{2+}+2NO_3^-+7K+3Na+3H]^{++}$	936.7334	936.7358

**Comparative study of interaction between 1,10-phenanthroline (*o*-phen) and Zn<sup>2+</sup>, Zr<sup>4+</sup> or Cd<sup>2+</sup>**

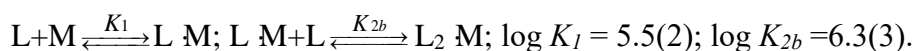
Under the same conditions, **TB(phen)** was insteaded with 1,10-phenanthroline for Zn<sup>2+</sup>, Zr<sup>4+</sup> or Cd<sup>2+</sup> binding property study via Uv-vis and fluorescence titrations.



**Figure S51.** Job plot corresponding to the interactions between *o*-phen and Zn<sup>2+</sup> in THF/CH<sub>3</sub>OH (1:1, v/v) at 298 K as monitored via Uv-vis spectroscopy. [Ligand] + [Metal] = 0.040 mM. Maximum value was seen at 0.5 in the case of Zn<sup>2+</sup>, this supports the 1:1 (ligand/metal) stoichiometry as suggested in the main text.



**Figure S52.** (a) Uv-vis spectra recorded for a solution of *o*-phen ( $1.00 \times 10^{-5}$  M in THF/CH<sub>3</sub>OH (1:1, v/v)) as a function of increasing Zn<sup>2+</sup> concentration (from 0 to 2.8 molar equiv) at 298 K. (b) The change in the absorbance at 270 nm (“■”) and the results of the corresponding nonlinear curve fitting according calculated model (red line) using Hyperquad 2003.<sup>12</sup> The equilibriums and related  $K_a$  calculation results as shown:



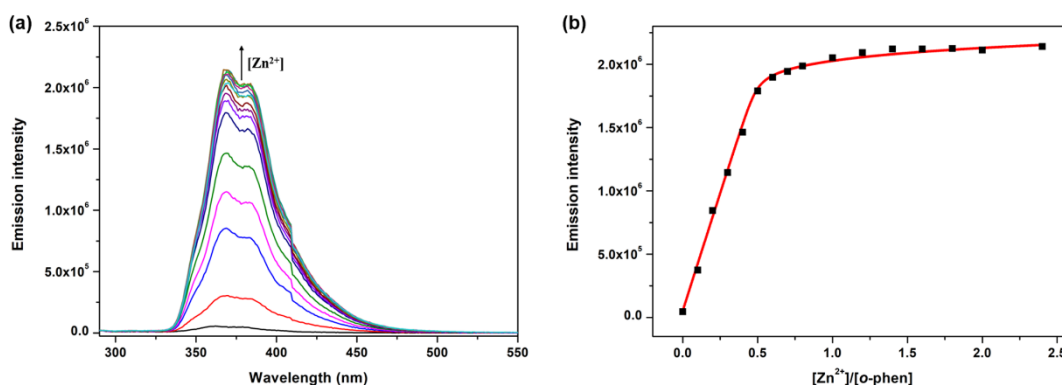


**Figure S53.** (a) Fluorescent emission spectra a solution of ***o*-phen** ( $1.00 \times 10^{-5}$  M in THF/CH<sub>3</sub>OH (1:1, v/v) with increasing Zn<sup>2+</sup> concentration (from 0 to 2.4 molar equiv) at 298 K. ( $\lambda_{\text{ex}} = 266$  nm, voltage = 400 V, entrance slit width = 5 nm, exit slit width = 8 nm) (b) The change in the fluorescence intensity at 370 nm (“■”) and the corresponding simulated emission intensity (red line). The equilibriums and related  $K_a$  calculations result as shown:

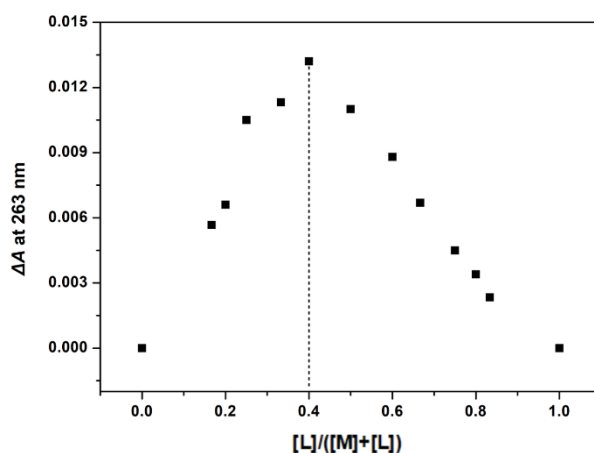


**Figure S54.** Job plot corresponding to the interactions between ***o*-phen** and Zr<sup>4+</sup> in THF/CH<sub>3</sub>OH (1:1, v/v) at 298 K as monitored via Uv-vis spectroscopy. [Ligand] + [Metal] = 0.040 mM. Maximum value was seen at 0.4 in the case of Zr<sup>4+</sup>, this supports the 1:1 and 1:2 (ligand/metal) stoichiometry as suggested in the main text.

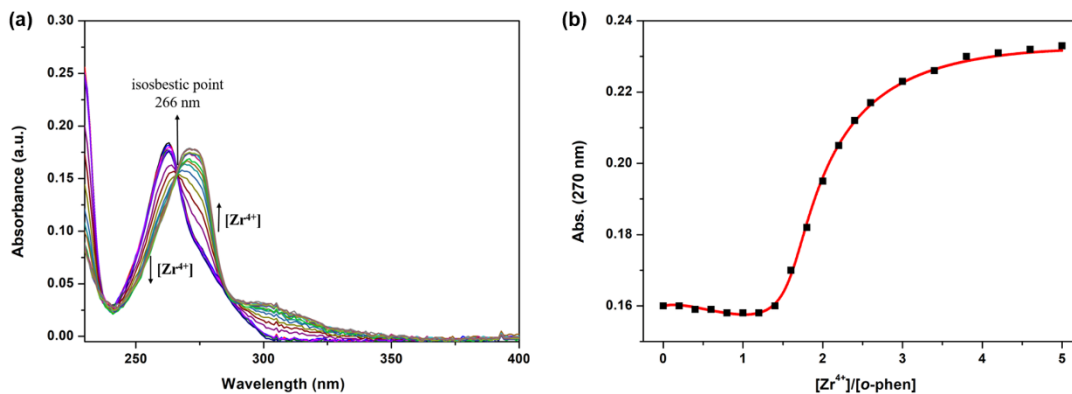


**Figure S55.** (a) Uv-vis spectra recorded for a solution of ***o*-phen** ( $1.00 \times 10^{-5}$  M in THF/CH<sub>3</sub>OH (1:1, v/v)) as a function of increasing Zr<sup>4+</sup> concentration (from 0 to 5.0 molar equiv) at 298 K. (b) The change in the absorbance at 270 nm (“■”) and the results of the corresponding nonlinear curve fitting according calculated model (red line) using Hyperquad 2003.<sup>12</sup> The equilibriums and related  $K_a$  calculation results as shown:

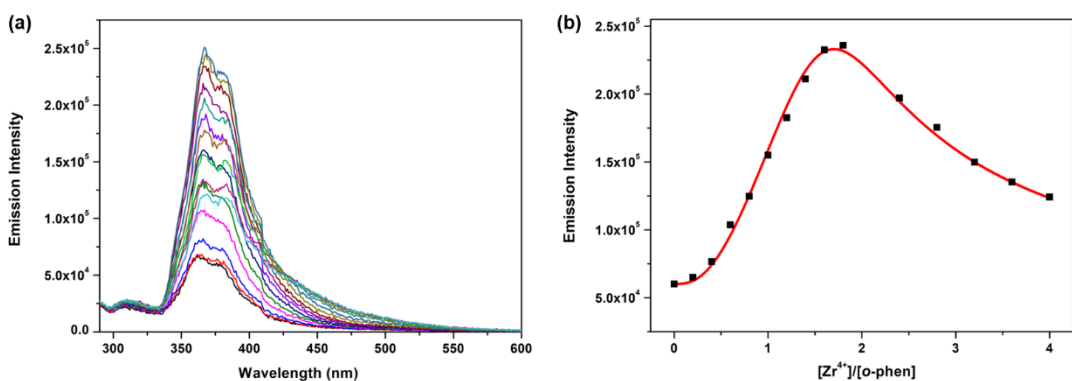


**Figure S56.** (a) Fluorescent emission spectra a solution of ***o*-phen** ( $1.00 \times 10^{-5}$  M in THF/CH<sub>3</sub>OH (1:1, v/v)) with increasing Zr<sup>4+</sup> concentration (from 0 to 4.0 molar equiv) at 298 K. ( $\lambda_{ex} = 266$  nm, Voltage = 400 V, entrance slit width = 5 nm, exit slit width = 8 nm) (b) change in the fluorescence intensity at 370 nm (“■”) and the corresponding simulated emission intensity (red line). The equilibriums and related  $K_a$  calculation results as shown:



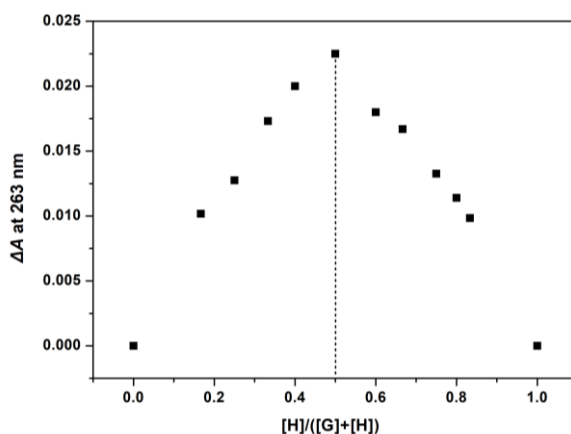


**Figure S57.** Job plot corresponding to the interactions between *o*-phen and Cd<sup>2+</sup> in THF/CH<sub>3</sub>OH (1:1, v/v) at 298 K as monitored via Uv-vis spectroscopy. [Ligand] + [Metal] = 0.040 mM. Maximum value was seen at 0.5 in the case of Zr<sup>4+</sup>, this supports the 1:1 (ligand/metal) stoichiometry as suggested in the main text.

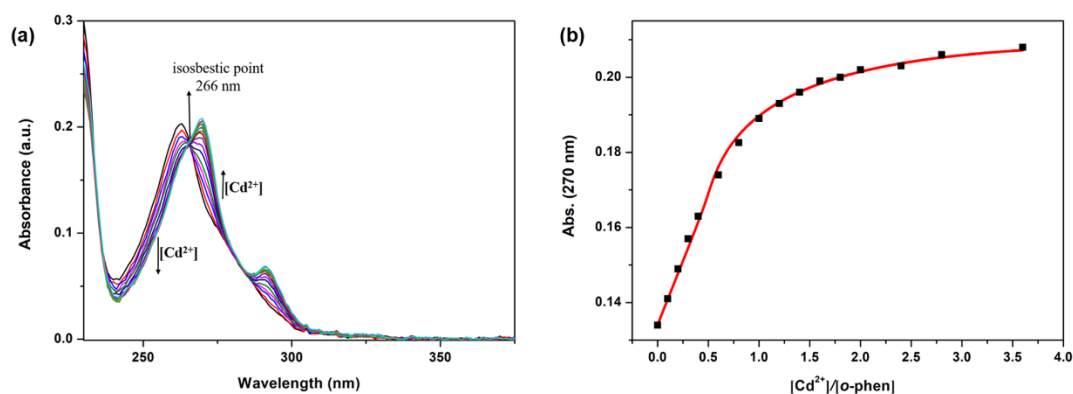


**Figure S58.** (a) Uv-vis spectra recorded for a solution of *o*-phen ( $1.00 \times 10^{-5}$  M in THF/CH<sub>3</sub>OH (1:1, v/v)) as a function of increasing Cd<sup>2+</sup> concentration (from 0 to 3.6 molar equiv) at 298 K. (b) The change in the absorbance at 270 nm (“■”) and the results of the corresponding nonlinear curve fitting according calculated model (red line) using Hyperquad 2003.<sup>12</sup> The equilibriums and related  $K_a$  calculation results as shown:  
 $L+M \xrightleftharpoons{K_1} L \cdot M$ ;  $L \cdot M+L \xrightleftharpoons{K_{2b}} L_2 \cdot M$ ;  $\log K_1 = 7.3(4)$ ;  $\log K_{2b} = 7.2(4)$ .

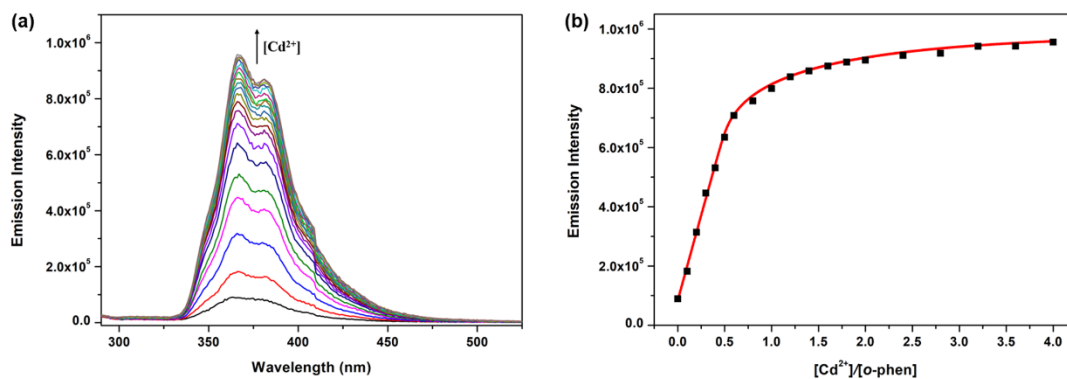


**Figure S59.** (a) Fluorescent emission spectra a solution of *o*-phen ( $1.00 \times 10^{-5}$  M in THF/CH<sub>3</sub>OH (1:1, v/v)) with increasing Cd<sup>2+</sup> concentration (from 0 to 4.0 molar equiv) at 298 K. ( $\lambda_{\text{ex}} = 266$  nm, Voltage = 400 V, entrance slit width = 5 nm, exit slit width = 8 nm) (b) change in the fluorescence intensity at 370 nm (“■”) and the corresponding simulated emission intensity (red line). The equilibriums and related  $K_a$  calculation results as shown:



**Section S4:** Single crystal X-ray diffraction analyses of  $[(\text{TB}(\text{phen}))_2\text{Cu}^+]\cdot\text{CF}_3\text{SO}_3^- \cdot \text{THF}$ ,  $[(\text{TB}(\text{phen}))_2\text{Ag}^+]\cdot\text{PF}_6^- \cdot \text{H}_2\text{O}$ ,  $[\text{TB}(\text{phen})\cdot\text{Cd}^{2+}\cdot(\text{NO}_3^-)_2] \cdot \text{CH}_3\text{OH}$

Single crystal samples of  $[(\text{TB}(\text{phen}))_2\text{Cu}^+]\cdot\text{CF}_3\text{SO}_3^- \cdot \text{THF}$ ,  $[(\text{TB}(\text{phen}))_2\text{Ag}^+]\cdot\text{PF}_6^- \cdot \text{H}_2\text{O}$  or  $[\text{TB}(\text{phen})\cdot\text{Cd}^{2+}\cdot(\text{NO}_3^-)_2] \cdot \text{CH}_3\text{OH}$  were cultivated via slow evaporation of the solution containing **TB(phen)** (2 mM) and 4 molar equiv of  $\text{CuCF}_3\text{SO}_3$ , 4 molar equiv of  $\text{AgPF}_6$  or 10 molar equiv of  $\text{Cd}(\text{NO}_3)_2$  in  $\text{THF}/\text{CH}_3\text{OH}$  (1:1, v/v).

**Table S3.** Single crystal X-ray diffraction data summary of  $[(\text{TB}(\text{phen}))_2\text{Cu}^+]\cdot\text{CF}_3\text{SO}_3^- \cdot \text{THF}$ ,  $[(\text{TB}(\text{phen}))_2\text{Ag}^+]\cdot\text{PF}_6^- \cdot \text{H}_2\text{O}$  and  $[\text{TB}(\text{phen})\cdot\text{Cd}^{2+}\cdot(\text{NO}_3^-)_2] \cdot \text{CH}_3\text{OH}$ .

	$[(\text{TB}(\text{phen}))_2\text{Cu}^+]\cdot\text{CF}_3\text{SO}_3^- \cdot \text{THF}$	$[(\text{TB}(\text{phen}))_2\text{Ag}^+]\cdot\text{PF}_6^- \cdot \text{H}_2\text{O}$	$[\text{TB}(\text{phen})\cdot\text{Cd}^{2+}\cdot(\text{NO}_3^-)_2] \cdot \text{CH}_3\text{OH}$
CCDC No.	2127679	2127693	2127694
description	block	prism	plate
color	green	red	dark orange
from solution	$\text{THF}/\text{CH}_3\text{OH}$	$\text{THF}/\text{CH}_3\text{OH}$	$\text{THF}/\text{CH}_3\text{OH}$
empirical formula	$\text{C}_{57}\text{H}_{36}\text{CuF}_3\text{N}_4\text{O}_4\text{S}$	$\text{C}_{52}\text{H}_{30}\text{AgF}_6\text{N}_4\text{OP}$	$\text{C}_{27}\text{H}_{18}\text{CdN}_4\text{O}_7$
<i>Mr</i>	993.50	979.64	622.85
crystal size (mm <sup>3</sup> )	$0.05 \times 0.03 \times 0.01$	$0.04 \times 0.02 \times 0.01$	$0.04 \times 0.03 \times 0.01$
Crystal system	triclinic	orthorhombic	Triclinic
Space group	P -1	F d d 2	P -1
a [Å]	9.7994(3)	15.6299(6)	8.5338(3)
b [Å]	13.3018(4)	56.8151(11)	11.7951(4)
c [Å]	17.3876(4)	37.3175(7)	12.6718(4)
$\alpha$ [deg]	76.769(2)	90.00	72.454(3)
$\beta$ [deg]	78.230(2)	90.00	71.768(3)
$\gamma$ [deg]	89.087(2)	90.00	86.420(3)
V/ [Å <sup>3</sup> ]	2158.79(11)	33138.5(16)	1154.39(7)
d/[g/cm <sup>3</sup> ]	1.528	1.571	1.792
Z	2	32	2
T [K]	169.99(10)	169.98(13)	170.00(12)
R1, wR2 $I > 2 \sigma(I)$	0.0469, 0.1254	0.0839, 0.2205	0.0220, 0.0485
R1, wR2 (all data)	0.0598, 0.1358	0.0943, 0.2342	0.0247, 0.0494
Quality of fit	1.035	1.006	1.003

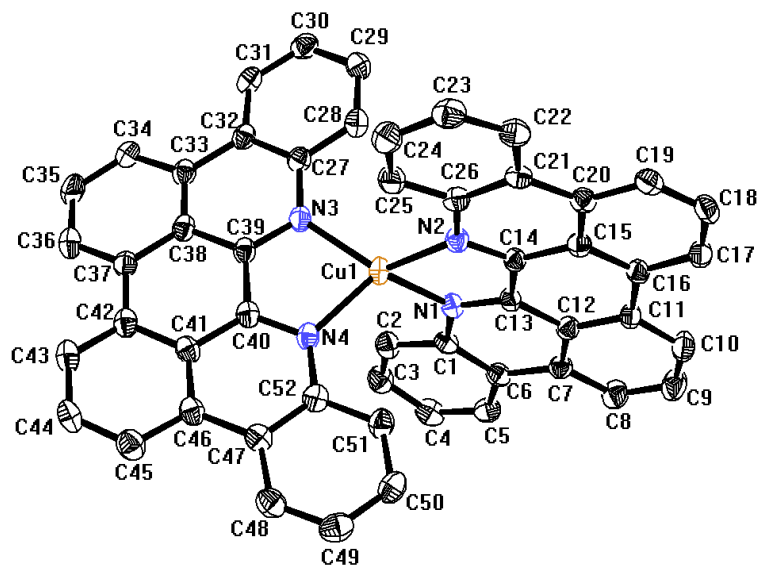


**Figure S60.** Ellipsoid form showing  $[(\text{TB}(\text{phen}))_2\cdot\text{Cu}^+]$  in the single crystal structure of  $[(\text{TB}(\text{phen}))_2\cdot\text{Cu}^+]\cdot\text{CF}_3\text{SO}_3^-\cdot\text{THF}$ . Displacement ellipsoids are scaled to the 50% probability level. All the other molecules and atoms have been omitted for clarity. Selected interatomic lengths (Å): Cu(1)...N(1) 2.02(2), Cu(1)...N(2) 2.01(1), Cu(1)...N(3) 2.01(0), Cu(1)...N(4) 2.03(0). Selected interatomic angles:  $\angle\text{N}(1)\dots\text{Cu}(1)\dots\text{N}(2)$  81.4(4)°,  $\angle\text{N}(1)\dots\text{Cu}(1)\dots\text{N}(3)$  130.3(1)°,  $\angle\text{N}(3)\dots\text{Cu}(1)\dots\text{N}(4)$  81.3(4)°,  $\angle\text{N}(2)\dots\text{Cu}(1)\dots\text{N}(3)$  127.1(1)°,  $\angle\text{N}(2)\dots\text{Cu}(1)\dots\text{N}(4)$  125.7(4)°,  $\angle\text{N}(1)\dots\text{Cu}(1)\dots\text{N}(4)$  117.0(4)°.

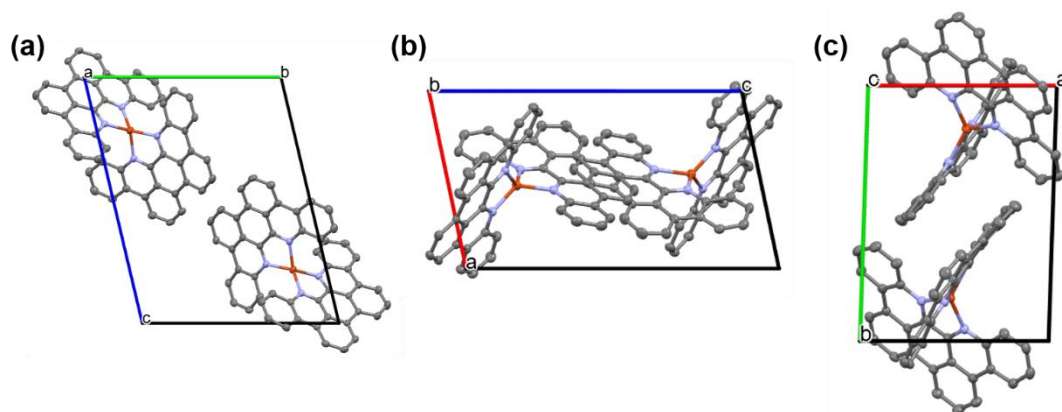


**Figure S61.** Packing diagram of  $[(\text{TB}(\text{phen}))_2\cdot\text{Cu}^+]$  in the single crystal structure of  $[(\text{TB}(\text{phen}))_2\cdot\text{Cu}^+]\cdot\text{CF}_3\text{SO}_3^-\cdot\text{THF}$  along with (a) *a*; (b) *b*; (c) *c* cell axis.

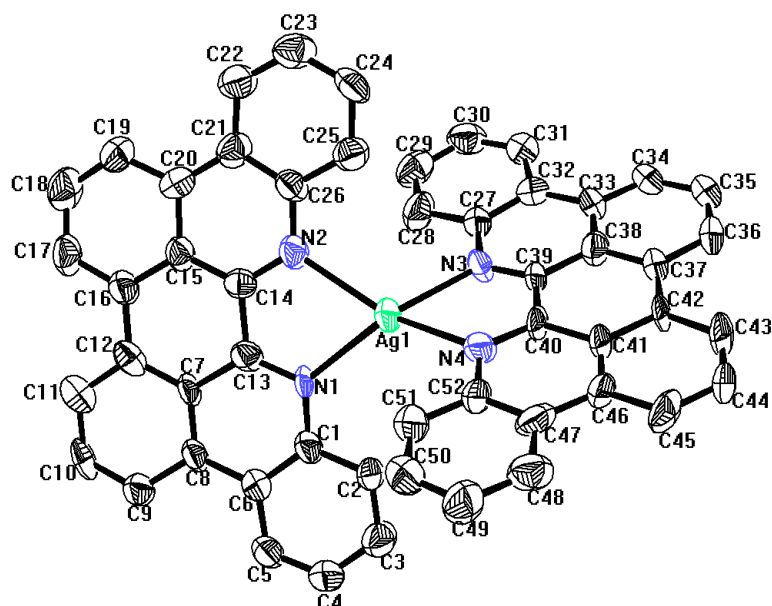


**Figure S62.** Ellipsoid form showing  $[(\text{TB}(\text{phen}))_2\cdot\text{Ag}^+]$  in the single crystal structure of  $[(\text{TB}(\text{phen}))_2\cdot\text{Ag}^+]\cdot\text{PF}_6^-\cdot\text{H}_2\text{O}$ . Displacement ellipsoids are scaled to the 50% probability level. All the other molecules and atoms have been omitted for clarity. Selected interatomic lengths (Å): Ag(1)...N(1) 2.30(1), Ag(1)...N(2) 2.35(1), Ag(1)...N(3) 2.34(1), Ag(1)...N(4) 2.36(1). Selected interatomic angles:  $\angle\text{N}(1)\dots\text{Ag}(1)\dots\text{N}(2)$  71.9(4)°,  $\angle\text{N}(1)\dots\text{Ag}(1)\dots\text{N}(3)$  143.6(4)°,  $\angle\text{N}(3)\dots\text{Ag}(1)\dots\text{N}(4)$  70.8(4)°,  $\angle\text{N}(2)\dots\text{Ag}(1)\dots\text{N}(3)$  114.2(4)°,  $\angle\text{N}(2)\dots\text{Ag}(1)\dots\text{N}(4)$  147.6(4)°,  $\angle\text{N}(1)\dots\text{Ag}(1)\dots\text{N}(4)$  124.5(4)°.

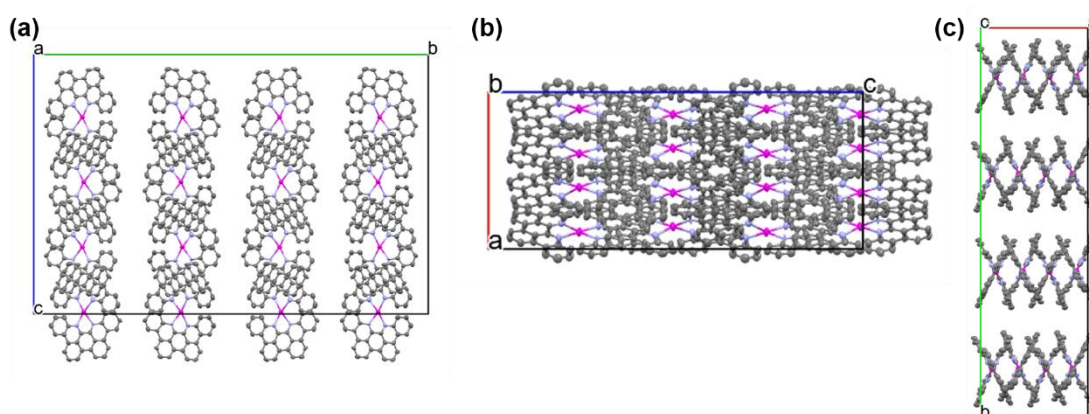


**Figure S63.** Packing diagram of  $[(\text{TB}(\text{phen}))_2\cdot\text{Ag}^+]$  in the single crystal structure of  $[(\text{TB}(\text{phen}))_2\cdot\text{Ag}^+]\cdot\text{PF}_6^-\cdot\text{H}_2\text{O}$  along with (a) *a*; (b) *b*; (c) *c* cell axis.

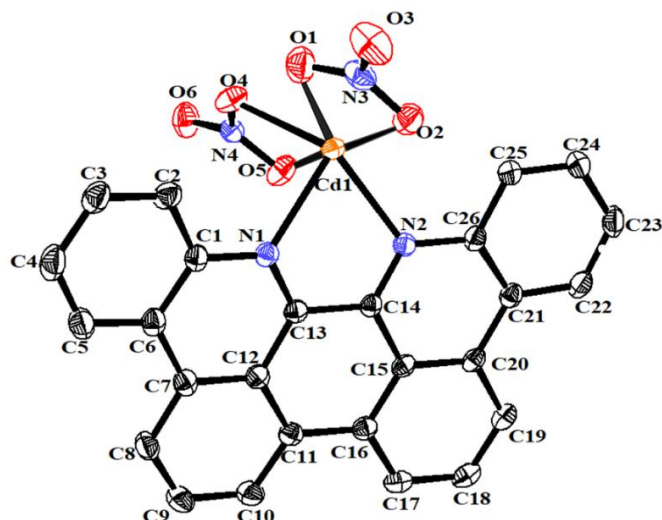


**Figure S64.** Ellipsoid form showing  $[\text{TB}(\text{phen})\cdot\text{Cd}^{2+}\cdot(\text{NO}_3^-)_2]$  in the single crystal structure of  $[\text{TB}(\text{phen})\cdot\text{Cd}^{2+}\cdot(\text{NO}_3^-)_2]\cdot\text{CH}_3\text{OH}$ . Displacement ellipsoids are scaled to the 50% probability level. All the other molecules and atoms have been omitted for clarity. Selected interatomic lengths (Å): Cd(1)...N(1) 2.33(4), Cd(1)...N(2) 2.30(3), Cd(1)...O(1) 2.39(4), Cd(1)...O(2) 2.39(4), Cd(1)...O(4) 2.34(4), Cd(1)...O(4) 2.61(4). Selected interatomic angles:  $\angle\text{N}(1)\dots\text{Cd}(1)\dots\text{N}(2)$  72.0(1)°,  $\angle\text{O}(1)\dots\text{Cd}(1)\dots\text{O}(2)$  53.6(0)°,  $\angle\text{O}(4)\dots\text{Cd}(1)\dots\text{O}(5)$  51.3(2)°,  $\angle\text{O}(1)\dots\text{Cd}(1)\dots\text{O}(4)$  81.8(4)°,  $\angle\text{O}(1)\dots\text{Cd}(1)\dots\text{O}(5)$  132.9(3)°,  $\angle\text{O}(2)\dots\text{Cd}(1)\dots\text{O}(4)$  134.5(4)°,  $\angle\text{O}(2)\dots\text{Cd}(1)\dots\text{O}(5)$  167.6(4)°,  $\angle\text{N}(1)\dots\text{Cd}(1)\dots\text{O}(5)$  79.3(3)°,  $\angle\text{N}(1)\dots\text{Cd}(1)\dots\text{O}(4)$  88.4(4)°,  $\angle\text{N}(2)\dots\text{Cd}(1)\dots\text{O}(2)$  91.6(1)°,  $\angle\text{N}(2)\dots\text{Cd}(1)\dots\text{O}(5)$  83.7(4)°,  $\angle\text{N}(2)\dots\text{Cd}(1)\dots\text{O}(4)$  133.9(2)°,  $\angle\text{N}(1)\dots\text{Cd}(1)\dots\text{O}(2)$  110.2(1)°,  $\angle\text{N}(1)\dots\text{Cd}(1)\dots\text{O}(1)$  105.9(3)°,  $\angle\text{N}(2)\dots\text{Cd}(1)\dots\text{O}(1)$  143.1(4)°.

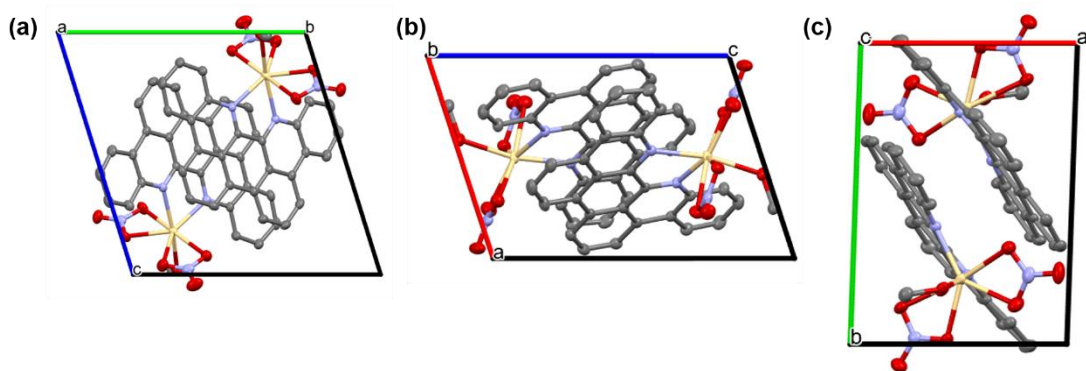


**Figure S65.** Packing diagram of  $[\text{TB}(\text{phen})\cdot\text{Cd}^{2+}\cdot(\text{NO}_3^-)_2]$  in the single crystal structure of  $[\text{TB}(\text{phen})\cdot\text{Cd}^{2+}\cdot(\text{NO}_3^-)_2]\cdot\text{CH}_3\text{OH}$  along with (a) *a*; (b) *b*; (c) *c* cell axis.

**Section S5: Protonation study of TB(phen) in CH<sub>2</sub>Cl<sub>2</sub>**

*General procedure for the Uv-vis and fluorescence spectral studies*

In this case, 2500  $\mu$ L of **TB(phen)** solution ( $1.00 \times 10^{-5}$  M in CH<sub>2</sub>Cl<sub>2</sub>) was added to quartz cell. The tested acid was trifluoroacetic acid (TFA,  $1.00 \times 10^{-3}$  M in CH<sub>2</sub>Cl<sub>2</sub>). All data were collected after each aliquot was added and mixed.

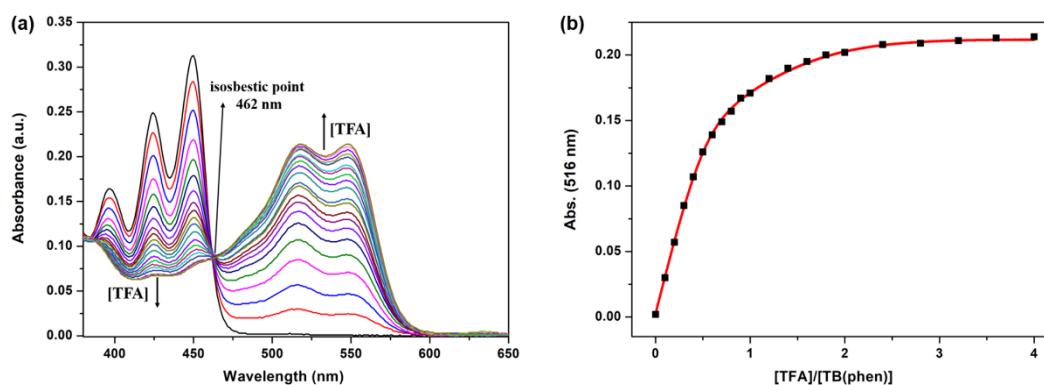


**Figure S66.** (a) Uv-vis spectra recorded for a solution of **TB(phen)** ( $1.00 \times 10^{-5}$  M in CH<sub>2</sub>Cl<sub>2</sub>) as a function of increasing TFA concentration (from 0 to 4.0 molar equiv) at 298 K. (b) The change in the absorbance at 516 nm (“■”) and the results of the corresponding nonlinear curve fitting according calculated model (red line) using Hyperquad 2003.<sup>12</sup> The equilibriums and related  $K_a$  calculation results as shown:  
 $L+H \xrightleftharpoons{K_1} L H$ ;  $L H+H \xrightleftharpoons{K_{2a}} L H_2$ ;  $L H+L \xrightleftharpoons{K_{2b}} L_2 H$ ;  $\log K_1 = 7.6(4)$ ;  $\log K_{2a} = 5.6(6)$ ;  $\log K_{2b} = 5.7(6)$ .

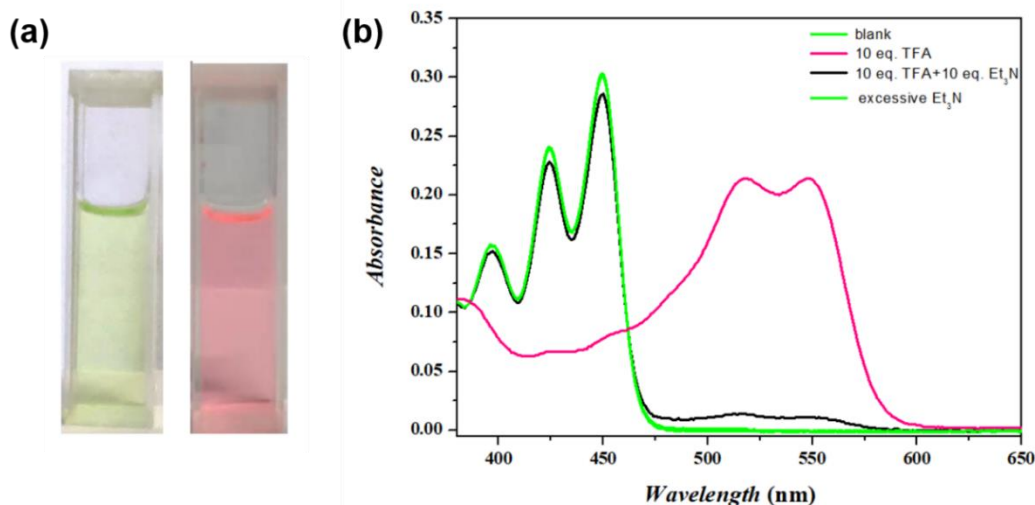


**Figure S67.** (a) The color change of **TB(phen)** solution when adding 2.0 molar equiv of TFA. (b) Uv-vis absorption of protonation of **TB(phen)** could be fully recovered by

adding same amount of trimethylamine and excess amount (10 molar equiv) of trimethylamine addition presented little change in the spectrum.

The process of interaction between **TB(phen)** and proton involves multiple chemical equilibria, the relevant equilibria equations are given in the following:

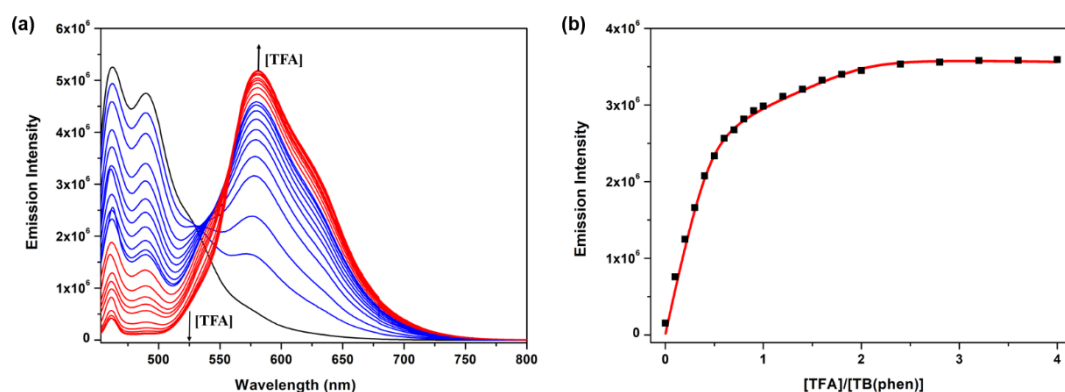
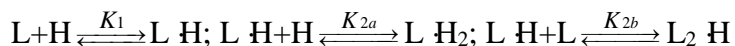
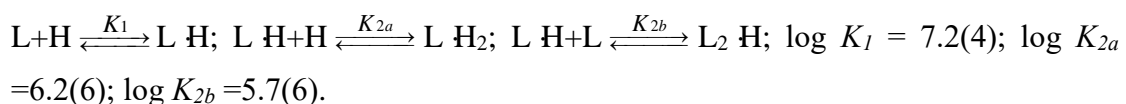


**Figure S68.** (a) Fluorescent emission spectra a solution of **TB(phen)** ( $1.00 \times 10^{-5}$  M in  $\text{CH}_2\text{Cl}_2$ ) with increasing TFA concentration (from 0 to 4.0 molar equiv) at 298 K. ( $\lambda_{\text{ex}} = 462$  nm, voltage = 400 V, entrance slit width = 5 nm, exit slit width = 8 nm) (b) The change in the fluorescence intensity at 620 nm (“■”) and the corresponding simulated emission intensity (red line). The equilibriums and related  $K_a$  calculation results as shown:



**Section S6:** Single crystal X-ray diffraction analysis of  $[\text{TB}(\text{phen})\cdot\text{H}^+]\cdot\text{CF}_3\text{SO}_3^-$

Single crystal samples of  $[\text{TB}(\text{phen})\cdot\text{H}^+]\cdot\text{CF}_3\text{SO}_3^-$  was cultivated via slow evaporation of the solution containing **TB(phen)** (2 mM) and 4 molar equiv of  $\text{Cu}(\text{CF}_3\text{SO}_3)_2$ , after 5 days, the single crystal was grown.

**Table S4.** Single crystal X-ray diffraction data summary of  $[\text{TB}(\text{phen})\cdot\text{H}^+]\cdot\text{CF}_3\text{SO}_3^-$

	$[\text{TB}(\text{phen})\cdot\text{H}^+]\cdot\text{CF}_3\text{SO}_3^-$
CCDC No.	2127695
description	prism
color	red
from solution	THF/CH <sub>3</sub> OH
empirical formula	C <sub>27</sub> H <sub>15</sub> F <sub>3</sub> N <sub>2</sub> O <sub>3</sub> S
<i>Mr</i>	504.47
crystal size (mm <sup>3</sup> )	0.04 × 0.02 × 0.01
Crystal system	monoclinic
Space group	P 21/c
a [Å]	6.8304(3)
b [Å]	12.7488(5)
c [Å]	24.0214(8)
α [deg]	90.00
β [deg]	95.584(3)
γ [deg]	90.00
V/ [Å <sup>3</sup> ]	2081.84(14)
d/[g/cm <sup>3</sup> ]	1.610
Z	4
T [K]	169.99(10)
R1, wR2 <i>I</i> > 2σ( <i>I</i> )	0.0476, 0.1193
R1, wR2 (all data)	0.0584, 0.1260
Quality of fit	1.035

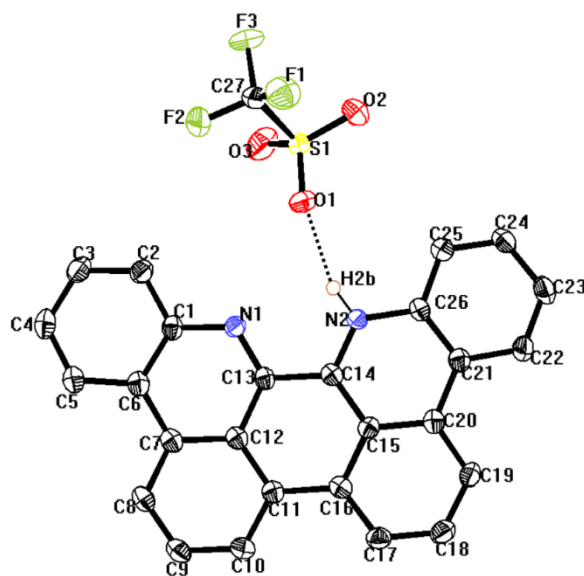


**Figure S69.** Ellipsoid form showing in the single crystal structure of  $[\text{TB}(\text{phen})\cdot\text{H}^+]\cdot\text{CF}_3\text{SO}_3^-$ . Displacement ellipsoids are scaled to the 50% probability level. Selected interatomic lengths (Å): O(1)...H(2b) 2.00(4), O(1)...N(2) 2.83(4). Selected interatomic angle:  $\angle\text{O}(1)\dots\text{H}(2b)\dots\text{N}(2)$  162.1(2)°.

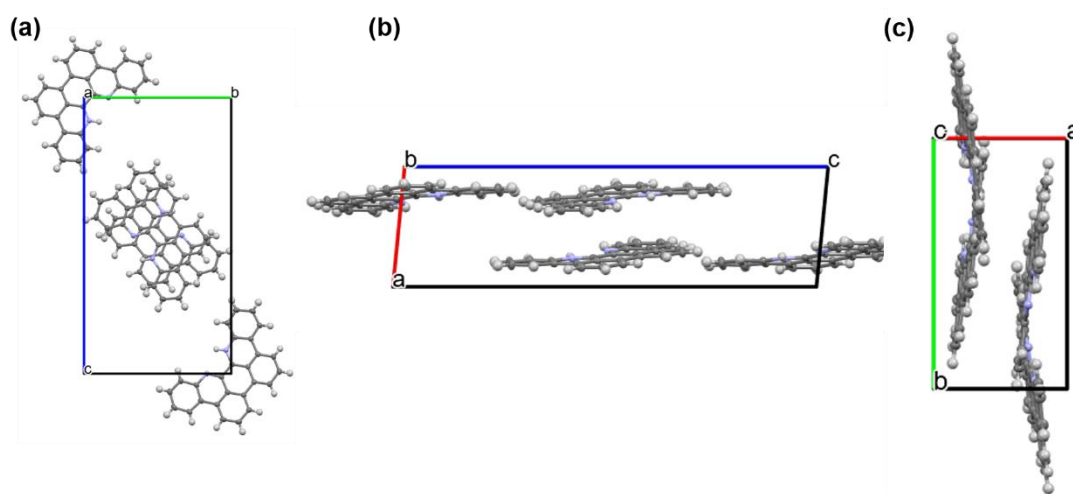


**Figure S70.** Packing diagram of  $[\text{TB}(\text{phen})\cdot\text{H}^+]$  in the single crystal structure of  $[\text{TB}(\text{phen})\cdot\text{H}^+]\cdot\text{CF}_3\text{SO}_3^-$  along with (a) *a*; (b) *b*; (c) *c* cell axis.

## Reference

- (1) H. E. Gottlieb, V. Kotlyar, A. Nudelman, *J. Org. Chem.*, 1997, **62**, 7512-7515.
- (2) G. M. Sheldrick, *SHELXL97*. Program for the Refinement of Crystal Structures, University of Göttingen, Göttingen, 1994.
- (3) O. V. Dolomanov, L. J. Bourhis, R. J. Gildea, J. A. K. Howard, *J. Appl. Cryst.*, 2009, **42**, 339-341.
- (4) G. M. Sheldrick, *Acta Cryst. A.*, 2015, **71**, 3-8.
- (5)  $R_w(F^2) = \{w(|F_o|^2 - |F_c|^2)^2/w(|F_o|^4)\}^{1/2}$  where w is the weight given each reflection.  $R(F) = (|F_o| - |F_c|)/|F_o|$  for reflections with  $F_o > 4(F_c)$ .  $S = [w(|F_o|^2 - |F_c|^2)/(n - p)]^{1/2}$ , where n is the number of reflections and p is the number of refined parameters.
- (6) A. J. C. Wilson, *International Tables for X-ray Crystallography. Vol. C, Tables 4.2.6.8 and 6.1.1.4*. Kluwer Academic Press, 1992.
- (7) (a) G. M. Sheldrick, *SHELXTL/PC (Version 5.03)*. Siemens Analytical X-ray Instruments, Inc., Wisconsin, **1994**. (b) L. J. Farrugia. *J. Appl. Cryst.*, 2012, **45**, 849-854.
- (8) L. G. Mercier, W. E. Piers and M. Parvez, Benzo- and Naphthoborepins: Blue-Emitting Boron Analogues of Higher Acenes, *Angew. Chem., Int. Ed.*, 2009, **48**, 6108-6111.
- (9) F. B. Mallory, K. E. Butler, A. C. Evans, E. J. Brondyke, C. W. Mallory, C. Yang, and A. Ellenstein, *J. Am. Chem. Soc.*, 1997, **119**, 2119-2124.
- (10) R. A. Pascal, Jr., D. V. Engen, B. Kahr and W. D. McMillan, *J. Org. Chem.*, 1988, **53**, 1687-1689
- (11) F. Colobert, V. Valdivia, S. Choppin, F. R. Leroux, I. Fernández, E. Álvarez and N. Khiar, *Org. Lett.*, 2009, **11**, 22, 5130-5133.
- (12) (a) K. A. Connors, *Binding Constants*. John Wiley and Sons, New York, 1987. (b) P. Gans and A. Sabatini, *A. Talanta*, 1996, **43**, 1739-1753.